VOLUME 85 NO. EM1
JANUARY 1959
PART 1

JOURNAL of the

Engineering Mechanics Division

PROCEEDINGS OF THE
AMERICAN SOCIETY
OF CIVIL ENGINEERS

Journal of the
ENGINEERING MECHANICS DIVISION
Proceedings of the American Society of Civil Engineers

CONTENTS

January, 1959

Papers

Journal of the
ENGINEERING MECHANICS DIVISION
Proceedings of the American Society of Civil Engineers

VORTEX FORMATION AND RESISTANCE IN PERIODIC MOTION[a]

J. S. McNown[1] M. ASCE and G. H. Keulegan

In two recent, independent studies,(1,2) closely related aspects of the resistance of a bluff body to the periodic motion of the surrounding fluid were investigated. In combination, the two studies provide a clear distinction between effects due to velocity and those due to acceleration as well as some insight into their variations during unsteady flow. Although indirect, the role of viscosity is paramount in that its consequences are separation, vortex formation and shedding, and resultant alterations of the virtual mass. The specification of these various aspects provides a basis for the correlation of theoretically predicted and observed forces.

The effects on resistance of the variation in size of a wake during unsteady flow has already been discussed in some detail.(2) A motion which starts from rest is initially irrotational and is free from separation. As the velocity increases, edge vortices form and grow into a wake. The completeness of the wake formation depends upon the comparative magnitudes of the duration of the unsteady flow and of the interval of time required for a wake to form, and upon the degree to which the body is streamlined.

If the form of the wake varies with time, the corresponding flow patterns and pressure distributions around the body vary. The forces attributable to velocity or to acceleration must then also change with time. Because both kinds of forces depend upon the state of development of the wake, they are in turn related to each other. For example, while the wake of a bluff body is small, the large curvatures of its boundary results in low pressures on the rear of the body and in a comparatively high coefficient of drag; simultaneously, the disturbance to the flow is less and the coefficient of mass is comparatively small.

Experiments at both the National Bureau of Standards and at the University of Michigan were planned to disclose the characteristics of resistance in unsteady flow. A standing wave was produced in an open tank so as to provide

Note: Discussion open until June 1, 1959. To extend the closing date one month, a written request must be filed with the Executive Secretary, ASCE. Paper 1894 is part of the copyrighted Journal of the Engineering Mechanics Division, Proceedings of the American Society of Civil Engineers, Vol. 85, No. EM 1, January, 1959.

a. Presented at the October 1957 ASCE Convention in New York, N. Y.

1. Dean, School of Eng. and Archt., Univ. of Kans., Lawrence Kans.

a two-dimensional oscillatory motion past a cylindrical body placed in the nodal plane of the wave. Thus, the flow varied from zero to a maximum in one direction, back to zero again, and then reversed direction, so that simple harmonic motion was closely approached. By varying the amplitude of the wave and the size of the body, one could obtain a motion with a comparatively small amplitude and negligible separation at one extreme and quasi-steady motion at the other. The resulting occurrences can be distinguished by means of a dimensionless frequency parameter $U_m T_o/D$, in which U_m represents the amplitude of velocity variation, T_o the period of the motion, and D the transverse dimension of the cylindrical body (measured normal to the direction of flow).

The work at the National Bureau of Standards was based on the equation of motion (see List of Symbols),

$$\frac{F}{L} = C_m \frac{\pi}{4} D^2 \rho \frac{dU}{dt} + C_D D \frac{\rho}{2} |U| U . \qquad (1)$$

This equation differs from that used in the Michigan study,

$$\frac{F}{L} = \frac{\pi D^2 \rho}{4} \left[k \frac{dU}{dt} + U \frac{dk}{dt} \right] + \frac{\rho V}{L} \frac{dU}{dt} + \frac{C_D D \rho |U| U}{2}, \qquad (2)$$

in two respects. The coefficient C_m combines the effects of pressure gradient and of inertia. Also, the effects of the term U dk/dt are absorbed, for Eq. (1), in the variation of C_m. The two equations differ conceptually in that different boundary conditions were assumed. Although no detailed integration was feasible in either case, the inner boundary for the contour integral was the surface of the body for Eq. (1), whereas the boundary was a surface enclosing both the body and its time-dependent wake for Eq. (2).

A final difference arose in the interpretations of experimental data in the two studies. In the first, an average value was obtained for a given occurrence by harmonic analysis of an entire cycle. In contrast, at Michigan the hypothesis was utilized that the value of k varied with time during each cycle because of its dependence upon the size of the wake. Accordingly, combination of the two methods of approach indicates only general trends in which average values are compared with instantaneous ones.

The free-streamline theory of Riabouchinski for flow around a flat plate was extended to provide a theoretical relationship between drag and virtual mass.(2) This resultant was used with an assumed variation of the virtual mass coefficient with time to calculate the cyclic variation of total force. Although evidently assumptive, the approach provided strong evidence of the importance of sizable and related variations of the coefficients of drag and virtual mass.

Results from experiment for flows past a thin flat plate and past a circular cylinder are presented in Fig. 1. In addition, the result from the free-streamline theory(2) is shown in Fig. 1a. In the two parts of Fig. 1, C_m is plotted against C_D. The points for the tests with the flat plate and the average curve for the cylinder were obtained by the elimination of the frequency parameter from Figs. 10-13 of the NBS study. The plot is striking evidence of the existence of unique relationships between the two parameters. Also, the theoretical result for the flat plate is a surprisingly good first approximation to the observed one.

Because time has been eliminated as a parameter in Fig. 1, the plots are one step removed from the physical occurrences. A half cycle begins at the

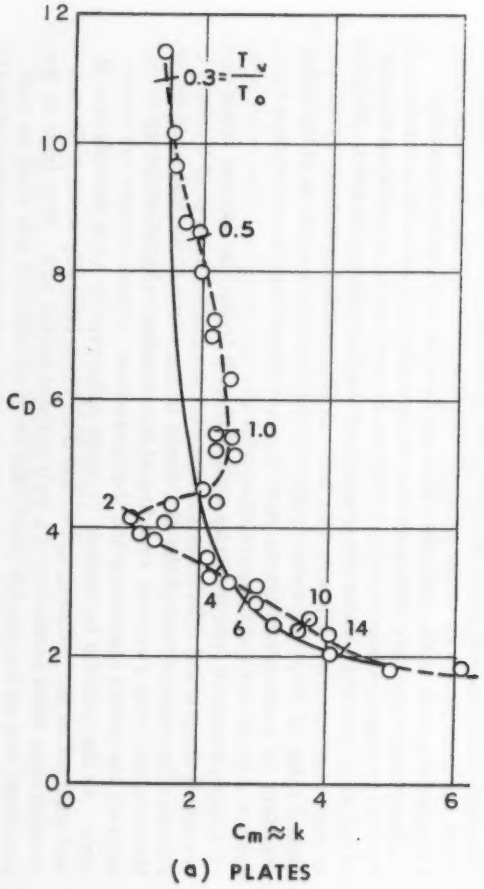

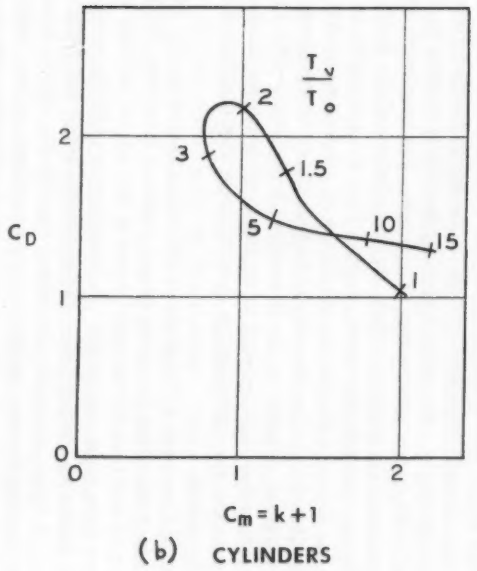

Fig. 1. Inter-relationship Between Coefficients of Drag and of Virtual Mass for (a) Flat Plates and (b) Circular Cylinders.

moment of zero ambient velocity corresponding to some point at the upper end of the extended curve in Fig. 1a. The ensuing occurrence is indicated by a partial traverse of the curve, the terminal point depending upon the relative duration of the half cycle, and a return along the same curve to the starting point. The process is duplicated for motion in the opposite direction during the second half of the cycle. The numbers indicate relative time in a dimensionless form described in a subsequent paragraph. Because each experimental point represents an average value, the variability of the coefficients during each cycle was undoubtedly even greater than it appears to be in Fig. 1.

Both parts of the figure indicate the existence of marked secondary effects which are ascribable to the formation and shedding of vortices and to the existence of vortices created in the preceding half-cycle. The interpreting of the graphical indication is somewhat presumptuous because the necessary concepts are still in the formative stage, and because the methods of analysis are yet to be fully tested.

Establishment of flow past a flat plate is greatly affected by the sharp edges which lead to separation for very small relative motions. Initially, a symmetrical pair of vortices forms and grows at the edges, so that regions of negative pressure also form and grow. In accordance with the predicted result, the smaller the vortices the lower the pressure along the downstream face of the plate. At first, these do not extend across the entire downstream face, as assumed for the theory, so that a more realistic curve would reach the limiting value of unity for C_m for some large but finite value of C_D.

If the cycle is sufficiently long, the symmetrical pattern becomes unstable and one of the vortices begins to grow more rapidly than the other, eventually becoming so large that it breaks away from the plate and moves downstream. During the period of growth, the vortex is still attached to the body, and C_m increases markedly as the composite body becomes fatter. Then, as the vortex is shed, the net form is again more sylph-like and the effective value of C_m decreases abruptly. Both trends are readily apparent in Fig. 1a as the two marked departures from the predicted monotonic curve. The shedding of other vortices produces comparable effects, but, because the data were averaged for each cycle, only the effect of the first is clearly delineated.

If motion in one direction persists long enough, in a relative sense (i.e., if C_mT/D is large), a succession of vortices is shed as for a taut wire singing in the wind—the well-known phenomenon of the Kármán vortex trail. The flow is then quasi-steady. The average value of C_D decreases toward the accepted value of about 2 for steady flow as the effective curvature of the wake boundary decreases, and the value of C_m increases with the increasing average size of the wake to a value of about 5.

Although Fig. 1b appears to be quite different from Fig. 1a, one consequence of the marked difference in geometry accounts for most of the disparity. The replacement of the sharpness of the edges of the flat plate by the comparatively generous rounding of the circular cylinder eliminates entirely the initial separation and the consequent regions of very low pressure. As the velocity increases, vortices subsequently form downstream of and adjacent to the cylinder, grow, and then move laterally so as to form a symmetrical wake composed of a well-defined vortex pair. Still later in the sequence, just as for the flat plate, one or more vortices are shed, so that an alternating vortex trail is established. This orderly progression is well documented by the photographic study of Prandtl.[3] The various portions of the loop in Fig. 1b are not as readily identifiable as were those in Fig. 1a,

partly because no theoretical result comparable to that for the flat plate is available. The minimum value of C_m occurs, as before, as the first vortex is shed. Also, because the vortices do not extend the disturbed region laterally, as they did for the plate, the value of C_m does not increase during the period of initial growth. The lower branch of the curve for the cylinder is comparable to the lower portion of the curve for the plate.

The extent to which vortices develop depends upon the duration of flow in one direction. More precisely, the ratio of this time interval to a time interval characteristic of vortex formation is a fundamental parameter. Use of the Strouhal number to indicate the time to form one vortex pair in a comparable steady flow is advantageous even for unsteady flow. Thus, the period T_O of the motion is some multiple (or fraction) of the period T_V of vortex shedding in steady flow at a velocity characteristic of the unsteady flow (e.g., the maximum velocity). If T_O/T_V is 0.1 or less, separation and vortex formation are relatively unimportant, the inertial effects being approximately those for the classical unseparated flow, and the velocity so small that the drag force is negligible. If the ratio is 10 or more, the motion becomes quasi-steady.

The numbers around the curves in Fig. 1 are values of T_O/T_V. In each case the complete period of motion is used (a full period for the wave, and the time for a pair of vortices to be shed). For several reasons, the numbers are 2 or 3 times as large as they should be to fit exactly the pattern described. The effective velocity is obviously less than the maximum, and the maximum occurs at the quarter-cycle. Vorticity from the preceding cycle noticeably retards the formation of the first vortex. Also, the instability which causes one vortex to be favored over the other of a pair may be slower to develop in flow which starts from rest than it is in steady turbulent flow. Whatever the cause, a study of motion pictures of the phenomenon confirmed the supposition that vortex formation is delayed for the periodic motion studied, and that the primary characteristics of the curve are directly related to the growth and shedding of the vortex as suggested in the preceding paragraphs in spite of the numerical disparity.

The foregoing concepts of resistance in unsteady motion are offered as a basis for further investigations. Its several shortcomings and uncertainties can be remedied only by the completion of additional studies. Significant progress should result from the evaluating of the effects of growing and moving vortices. These are predictable from classical theory, and can be correlated with measured forces. Studies should be devised to test and to extend these concepts so as to interpret rather than merely to describe the effects of unsteadiness. So many kinds of unsteady flow are possible that a wholesale empirical solution is impracticable. The separation of the effects of velocity and of acceleration, the designation of the relative time scale appropriate to the phenomenon, and the definition of the role of vortex formation are essential to an understanding of the occurrence.

List of Symbols

F/L	force per unit length of cylindrical body
C_m	inertial coefficient (including term for pressure gradient)
D	width of cylindrical body (normal to direction of flow)

ρ	mass density of the fluid
U	velocity of fluid
C_D	coefficient of drag
k	coefficient of virtual mass (not including term for pressure gradient)
V/L	volume per unit length of cylindrical body

REFERENCES

1. Keulegan, G. H., and Carpenter, L. H., "Forces on Cylinders and Plates in an Oscillating Fluid," Natl. Bur. Std. Rep. 4821, U.S. department of Commerce, Sept., 1956.
2. McNown, J. S., "Drag in Unsteady Flow," Proc. IX Int. Cong. Appl. Mech., Brussels, 1957.
3. Prandtl, L., and Tietjens, O. G., Applied Hydro- and Aeromechanics, New York, McGraw-Hill, 1934.

Journal of the
ENGINEERING MECHANICS DIVISION
Proceedings of the American Society of Civil Engineers

APPLICATIONS OF ELECTRICAL ANALOGS OF STATIC STRUCTURES

Frederick L. Ryder[1]

SYNOPSIS

A previous paper(1) has dealt with electrical analogs which are based on certain similarities between elastic energy in structures and power in electrical networks, and in which current is used to simulate forces and moments in the structure, and voltage to simulate deflections and slopes. The work is continued here in the following respects:

1. Treatment of 3-dimensional frames.
2. Treatment of structures containing members which are non-linear, either by reason of a non-linear stress-strain curve for the material or because the deflections are large enough to significantly alter the equilibrium relationships among the forces and moments.
3. A practical method of setting up analog circuits.
4. Partition of complicated structures to permit simulation by an analog device with a limited number of electrical components.
5. Applied deflections and thermal effects.
6. Experimental work.

NOTATION

The letter symbols adopted for use in this paper are defined where they first appear, in the illustrations or in the text, and are arranged alphabetically, for convenience of reference, in the Appendix. Except for new symbols introduced herein, the notation is the same as in the companion paper.(1)

Note: Discussion open until June 1, 1959. To extend the closing date one month, a written request must be filed with the Executive Secretary, ASCE. Paper 1895 is part of the copyrighted Journal of the Engineering Mechanics Division, Proceedings of the American Society of Civil Engineers, Vol. 85, No. EM 1, January, 1959.

1. Member Scientific Research Staff, Republic Aviation Corp., Farmingdale, N. Y.

INTRODUCTION

The basic approach followed by the writer in devising electrical analogs for static structures has been explained in the Introduction of the companion paper.[1] Since the writing of that paper other works on the subject have appeared.[2] In general, however, these are based on the following considerations:

1. Force and moment equilibrium in the structure is simulated by current-continuity requirements in the analog.
2. Deflection and slope changes in each member are simulated by voltage differences.
3. Compatibility of slopes and deflections in the structure is simulated by compatibility of voltages in the analog.

Hence these papers do not deal with structural energy and electrical power explicitly, except possibly to make use of the former in evaluating the deflection and slope values needed in step 2 above. By contrast, in this and the companion paper[1] the second and third of the above considerations are completely ignored, and instead the following requirement is met:

4. The elastic energy is simulated by half the electrical power.

The consequence of meeting requirements 1 and 4 alone can be realized by comparing Castigliano's well-known theorems with their electrical equivalents[3] which have been described in the companion paper, as follows:

Castigliano's Theorems	Electrical Equivalents
1. Forces and moments are such as to minimize the elastic energy, subject to equilibrium requirements.	1. Currents are such as to minimize the electrical power, subject to requirements of current-continuity.
2. The deflection (or slope) at a given point is the derivative of the elastic energy with respect to a corresponding force (or moment) applied to the point.	2. The voltage at a given point is the derivative of half the electrical power with respect to a current supplied to this point.

As a result of the first of the above laws (often called the principle of least work in the structural case) the forces and moments take on definite values, and the currents take on corresponding values. As a result of the second law (often designated simply as Castigliano's Theorem in the structural case) the deflections and slopes at all points take on definite values, and the voltages take on corresponding values. Thus by measuring the voltages in the analog one can evaluate the deflections and slopes in the structure, even though deflections, slopes and voltages were not considered explicitly (in steps 2 and 3 above) in setting up the analog.

The companion paper deals with the analogs for a number of illustrative types of structures. The present paper treats various topics which were left out of the previous paper in order to keep it at an introductory level, or because the material had not been developed at the time that paper was written.

3-Dimensional Frame

A general treatment of the electrical analog for the 3-dimensional frame is too lengthy for inclusion here but may be found in the thesis[4] on which this paper is partly based. Instead we shall investigate a single specific case, which however displays most of the features of interest.

Fig. 1(a) shows three orthographic projections of a rigidly connected frame in which the cross-section is constant in any one member, and which is loaded by force F and completely restrained with respect to moment (including torsion) and force at support points 1 and 4. Fig. 1(b) shows an oblique projection of the frame and defines the coordinate axes x, y, and z, and also shows the three unknown forces and three unknown moments at each of the two support points. The moments are indicated by circled arrows, each of which denotes the direction of advance of a right-hand screw rotated by the moment. There are a total of twelve unknown reactions and six equations of equilibrium of the overall structure (three force equations and three moment equations), so that it is indeterminate to the sixth degree.

In developing the analog we shall make use of the basic moment analog shown in Fig. 4(c) of the companion paper,[1] and reproduced here as Fig. 2(b) and in abbreviated symbolic form as Fig. 2(c). The corresponding structural member is shown in Fig. 2(a), where for our present purpose it may be considered that the shear S and the respective applied end-moments M_{BH} and M_{HB} lie in the plane of the paper. It is seen by inspection that the equation of moment equilibrium of the beam is simulated by current-continuity requirements in the analog, and it has been shown in connection with Eq. (15) in the companion paper[1] that the electrical power dissipation (with the transformer assumed ideal) will equal twice the bending work if

$$\rho = L/EI \qquad (1)$$

where E is the modulus of elasticity, I is the flexural moment of inertia of the beam cross-section, and the expression on the right is the bending compliance, or change of slope per unit constant moment in the beam. (It is assumed that the work associated with direct shear and with any tension which may exist in the beam is negligible.) It has also been shown, as a consequence of Castigliano's Theorem and its electrical equivalent, that the voltage drop from B to H in Fig. 2(b) represents the increase of slope between B and H caused by bending, and the voltage drop from B to O represents $1/L$ times the bending deflection of H from the line tangential to the beam at B, in the direction of positive shear; and correspondingly for the voltage drop from H to O.

The analog of Fig. 1 is shown in incomplete form in Fig. 3. It is divided into three more or less separate networks, as indicated by the horizontal dot-dash lines, dealing essentially (but not exclusively) with x-, y-, and z-moments respectively, as distinguished by the direction of the circled arrows in Fig. 1(b). First considering member 1-2, we ground point 1 in all three networks to simulate zero values of x-, y-, and z-slope,* and designate the values of current leaving the networks at these points to correspond with the

*Slope is here defined as the elastic rotation in the direction of a given component of moment, regardless of whether the rotation arises from flexure or torsion.

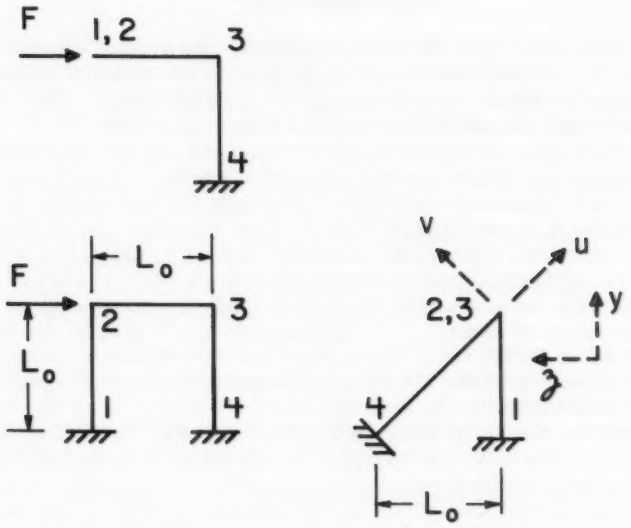

(a) orthographic projections

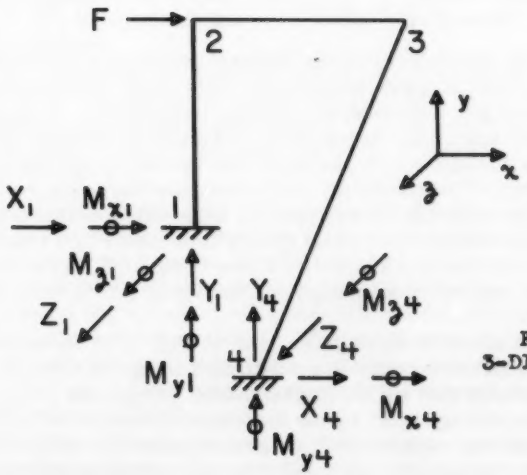

Fig. 1
3-DIMENSIONAL FRAME

(b) oblique projection

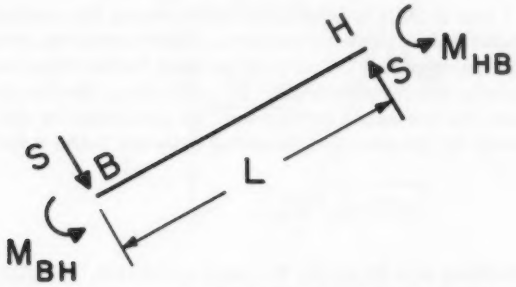

(a) structural member

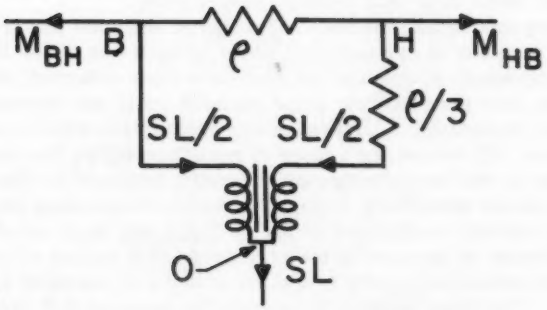

(b) moment analog

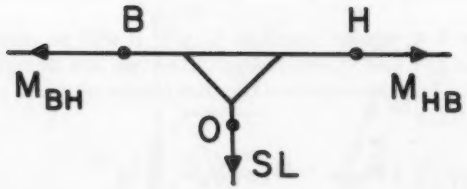

(c) symbolic form of moment analog

Fig. 2 BASIC MOMENT ANALOG

corresponding unknown reaction moments defined in Fig. 1(b). Moment M_{x1} causes bending in member 1-2, and the value of x-moment increases by the amount $-Z_1L_o$ between 1 and 2; this is taken care of by using the analog shown in Fig. 2(c), with a suitable value of shear current. Corresponding considerations hold for z-moment in member 1-2 acts in torsion rather than bending, the torsional moment having the constant value M_{y1} all along the member. It is easy to show that twice the torsional energy will be simulated by the electrical power dissipated in the resistor inserted between 1 and 2 in the y-network if

$$\rho_{y12} = L_o/GI_T \qquad (2)$$

where G is the shear modulus and I_T is the moment of inertia, effective in computing torsional deflection, of the beam cross-section. The voltage drop across this resistor in the direction from 1 to 2 is then the increase of y-slope, which corresponds with the fact that the voltage drops from 1 to 2 in the x- and z-networks refer to x- and z-slope respectively.

In using the bending analog for member 1-2 we have assumed that the cross-section of the member is symmetrical about at least one of the two axes to which the components of bending moment have been referred, in this case the x and y axes, else the resulting slope changes could not necessarily have been determined separately; a corresponding assumption will be made for the other members. Of course the values of resistors within the moment analogs corresponding to the two components of bending moment for the given member will depend on the values of I referred to the corresponding axes.

By inspection the currents designated as M_{x23}, M_{y23} and M_{z23} equal the corresponding components of moment in the structure (as a matter of definition, M_{x23} is the component of moment, applied to end 2 of member 2-3, referred to the x-axis). The three electrical analogs for member 2-3 are next developed as before; the x-moment produces torsion and the y- and z-moments produce bending, the increase in bending moment being Z_1L_o and $-Y_1L_o$ respectively. The moments M_{x34}, M_{y34} and M_{z34} then represent corresponding components of moment applied to member 3-4 at 3, and the voltage of point 3 in the three networks, measured below ground, represents the corresponding component of slope.

In dealing with member 3-4, whose length is $L_o\sqrt{2}$, it will be convenient to refer the moments to axes x, u and v, where the latter two are designated by dotted arrows in Fig. 1(a). For convenience the directions of y and z are also shown. We may write:

$$\left.\begin{aligned} M_{u34} &= (M_{y34} - M_{z34})/\sqrt{2} \\ M_{v34} &= (M_{y34} + M_{z34})/\sqrt{2} \end{aligned}\right\} \qquad (3)$$

Moment M_{x34} produces bending, and the corresponding increase in moment between 3 and 4 is $(Y_1 + Z_1)\,L_o$; this is taken care of in Fig. 3 by a moment analog as before. M_{u34} is a torsional moment, and is handled (within the y-network for convenience) by a single resistor as before; the means of developing the current M_{u34} will be dealt with later. M_{v34} is a bending moment with a corresponding increase of $-\sqrt{2}(F + X_1)L_o$ along the member, and is handled accordingly. Points 4 are grounded in all networks to simulate zero slope,

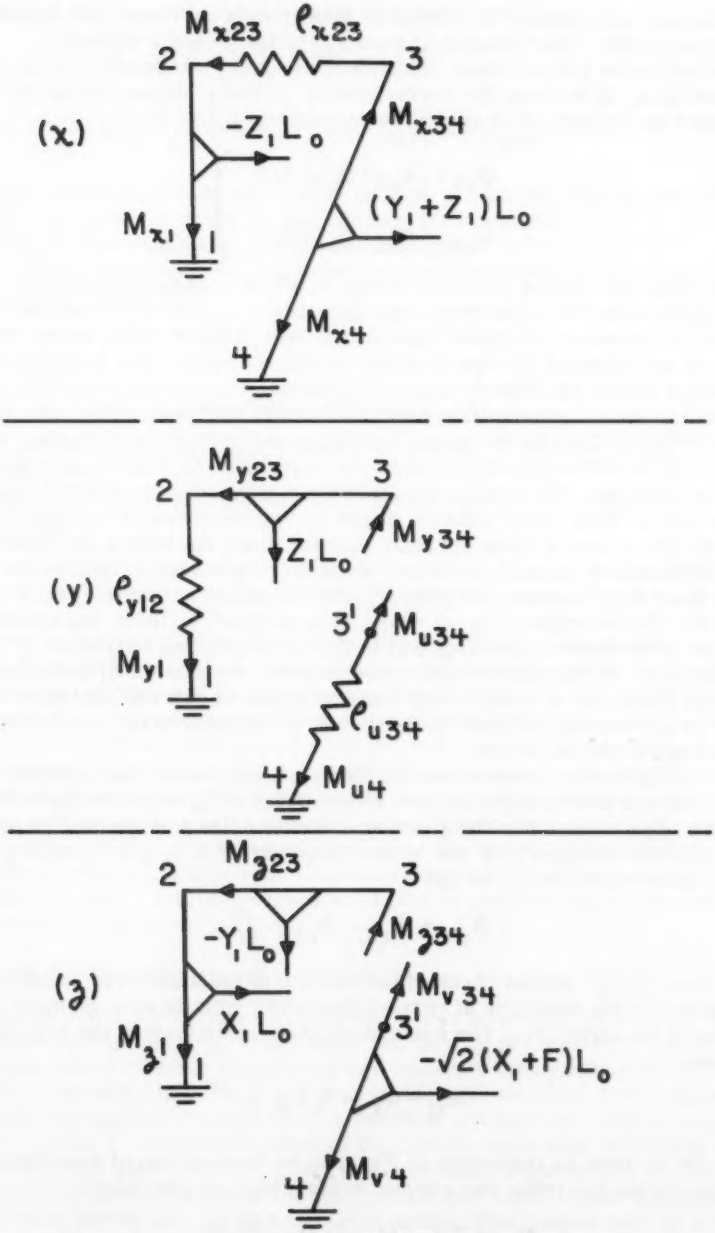

Fig. 3 ANALOG FOR Fig. 1 (incomplete)

and the currents leaving the circuit at these points correspond to applied reaction moments. The voltages at points 3' in the y- and z-networks, measured below ground, must simulate the u- and v-slopes of point 3, namely θ_{u3} and θ_{v3}. If desired, the corresponding y- and z-slopes can be determined as follows, as is evident by inspection of Fig. 1(a):

$$\left.\begin{aligned} \theta_{y3} &= (\theta_{v3} + \theta_{u3})/\sqrt{2} \\ \theta_{z3} &= (\theta_{v3} - \theta_{u3})/\sqrt{2} \end{aligned}\right\} \tag{4}$$

The complete analog is shown in Fig. 4, which is obtained from Fig. 3 by inter-connecting the leads previously left open in a manner compatible with the indicated values of current assumed to flow in those leads, using transformers and external current-generators as necessary. The primary and secondary of any one transformer are designated by circles connected by a dotted line as in the companion paper,(1) and the required turns ratio (including polarity) is fixed by the ratio of primary and secondary currents. Any scheme of connection which satisfies the designated currents is acceptable with this proviso: the various currents simulating any one unknown force or moment must be so inter-related, either by transformers or by direct connection, that if one of these currents is determined the others are fixed by considerations of current-continuity alone (here extended to include the effect of the fixed ratio between the primary and secondary currents of each transformer). For example, current $-Z_1L_o$ at point Q is related to the current Z_1L_o at P by direct connection, and to the corresponding current at R by a transformer. If this transformer were omitted, the number of redundant currents (those not determined by considerations of current-continuity alone) would be greater by one than the number of redundants in the structure, and the analogy would be invalid.

By Castigliano's Theorem and its electrical equivalent, the voltages at Q and O, measured below ground, are respectively $1/L_o$ times the deflections δ_{z2} and $-\delta_{x2}$ of joint 2 in the z and -x directions (the y-deflection is zero). Similarly, the voltages at P and P' are respectively $1/L_o\sqrt{2}$ times δ_{v3} and $-\delta_{x3}$. Since δ_{u3} is zero, we have

$$\delta_{y3} = \delta_{z3} = \delta_{v3}/\sqrt{2} \tag{5}$$

An easy though partial check of the validity of the analog can be obtained by comparing the equations of current-continuity with those of moment equilibrium in the structure. The summation of currents leaving the x-portion of the analog is:

$$M_{x1} + M_{x4} + Y_1 L_o = 0$$

which can be seen by inspection of Fig. 1 to be the equation of x-moment equilibrium. In the y-portion two current summations may be taken:

$$M_{y1} + Z_1 L_o - M_{y34} = 0 \tag{6}$$

$$M_{u4} + M_{y34}/\sqrt{2} - M_{z34}/\sqrt{2} = 0 \tag{7}$$

whereas in the z-portion the following two may be taken:

$$M_{z1} + (X_1 - Y_1) L_o - M_{z34} = 0 \tag{8}$$

$$M_{v4} - \sqrt{2}(F + X_1) L_o + M_{y34}/\sqrt{2} + M_{z34}/\sqrt{2} = 0 \tag{9}$$

M_{y34} and M_{z34} may be eliminated by Eqs. (6) and (8), and M_{u4} and M_{v4} may be expressed in terms of M_{y4} and M_{z4} by inspection of Fig. 1. When the resulting substitutions are incorporated in Eqs. (7) and (9), and these equations are successively added together and then subtracted one from the other, there is obtained:

$$M_{y1} + M_{y4} + (Z_1 - F - X_1) L_o = 0$$

$$M_{z1} + M_{z4} - (F + Y_1) L_o = 0$$

which are seen to be the equations of equilibrium of y- and z-moment respectively.

Experimental work in connection with this example is discussed elsewhere in this paper.

Non-Linear Structures

Non-linearity in structures may be divided into two general classes: the first one arises from a non-linear relationship between stress and strain, and includes the case where the stress-strain relationship is not unique but depends on the previous loading history. Important applications of this occur in structures which are still useful after the material has passed beyond the elastic limit but before complete destruction has taken place, as in bomb shelters. In the second class the stress-strain relationship may be linear, but the deflections are large enough to significantly alter the equilibrium relationships among the forces and moments. The most familiar case is the structural column, in which the transverse deflections, though small, act in conjunction with a relatively large axial load to produce appreciable and sometimes disastrous moment.

Non-Linear Stress-Strain Relationship

In a pin-connected truss this may be treated by preparing for each member a curve of compliance vs. axial force, and then by successive iteration finding such values of those resistors which simulate the compliance (as in Fig. 1 of the companion paper[1]) as are compatible with the axial force values. As a practical matter the compliance is known in advance for relatively light loads, so that a convenient method of procedure starts with the analog set for light load, the latter then being increased in small steps so that the successive adjustments in the resistors are small and hence relatively independent of each other during any one step of the iteration. The method may be extended to vary the load (in small steps) according to any desired loading program, which is useful when the compliances depend on the loading history.

In a structure containing bending members the situation is much more complicated. Considering only the 2-dimensional case, we note that the

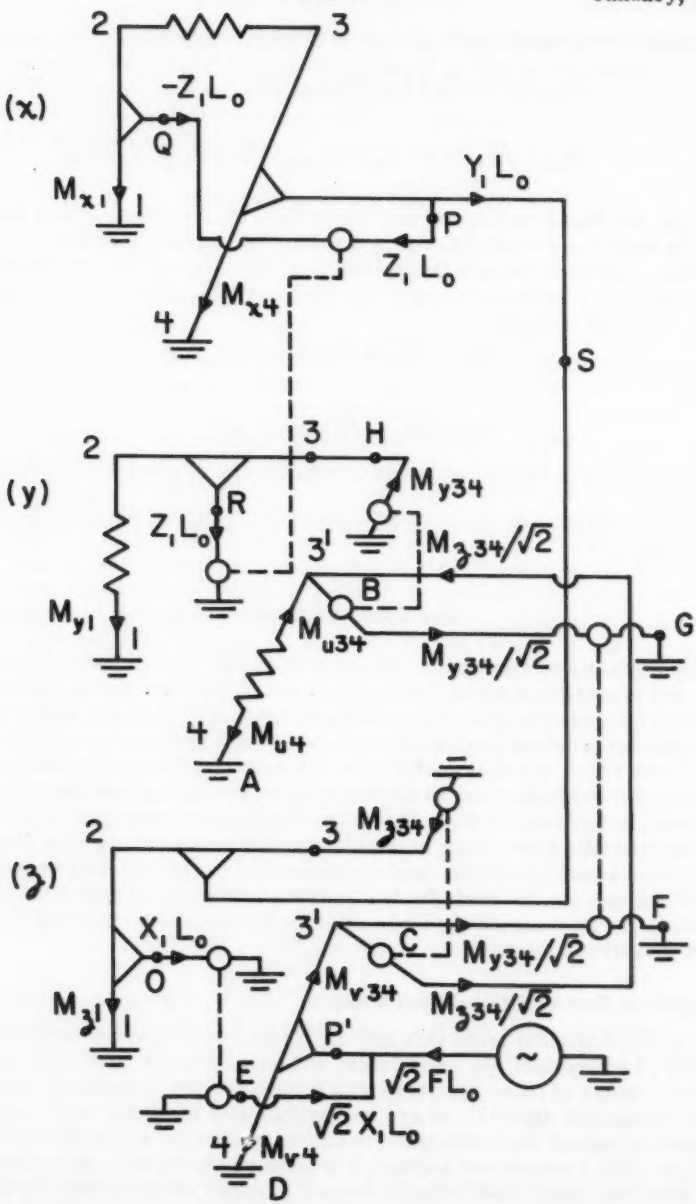

Fig. 4 ANALOG FOR Fig. 1 (complete)

change of slope θ_{BH} along the member in Fig. 2(a), as well as the deflection δ_{BH} at H measured normal to the tangent through B are functions[5] of both M_{BH} and S. For any values of these two parameters the horizontally-disposed resistor in Fig. 2(b) can be adjusted so that its voltage drop simulates θ_{BH}, and the vertically-disposed resistor may be adjusted so that the voltage drop from B to O simulates δ_{BH}/L. As in the previous case, it is well to start the analog at light load and to change the load in small steps.

Non-Linearity Due to Effect of Deflections on Equilibrium Relationships

This occurs in individual compressive members in rigid frames and trusses, and in practically all members of long slender trusses subjected to forces which tend to place the structure as a whole in compression, as in derrick-boom trusses. In individual column-like members it is often possible to neglect the extra deflections and slopes due to column effect until the load is large enough to cause column failure. On the other hand, when the entire truss acts as a column the effect of the deflections on the force-equilibrium equations may have to be considered. As a highly simplified example consider the pin-connected truss of Fig. 5(a), where it is assumed that the structure as a whole is adequately restrained against column buckling outside of its plane, and that individual compressive members have no appreciable column instability. Conditions of symmetry permit us to split the truss along the longitudinal axis of member 3-4, and to consider the left half-truss supported against x- and y-deflections at joint 3 and against x-deflection at 4. The x- and y-networks of the electrical analog, shown in Fig. 5(b), are developed in the same manner as in Fig. 2 of the companion paper.[1] With the changes of slope of the various members caused by the relatively small x- and y-components of deflection taken into account, the transformer turns ratios must be such as to impose suitable ratios between the x- and y-components of tensile force in any member.

The procedure is to first set the transformer turns ratios with the deflections assumed to be zero, find the resulting deflections by measurement of the analog, and then compute new values of the turns ratios. Successive runs are taken until the solution converges, or (if the truss is unstable) diverges. However, the transformer voltage drops can be expected to be relatively very large since they have been shown to represent x- and y-components of branch deflection due to branch rotation, which are relatively very large in a compressively-loaded shallow truss. Hence errors due to transformer imperfections (discussed in greater detail below) will be unduly large, and the analog is not recommended for this type of application.

Practical Method of Setting up Analog Circuits

In the case of complicated structures it is convenient to have a relatively systematic method for setting up the analog circuit. A procedure suitable in many practical cases is described in the following steps in connection with the 2-dimensional rigid frame of Fig. 6, where it is assumed for simplicity that cross-sections are constant, and that the elastic energy associated with direct shear and tension is negligible compared to the bending energy.

1. Designate each joint by a letter rather than by a number; this will simplify the clerical aspects of the work. For structures with many

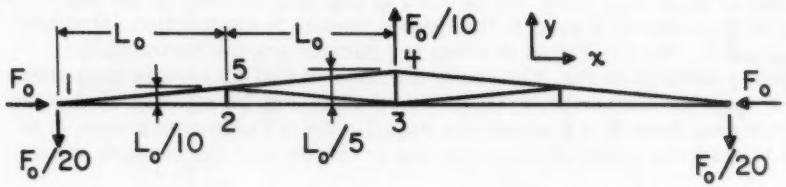

(a) truss

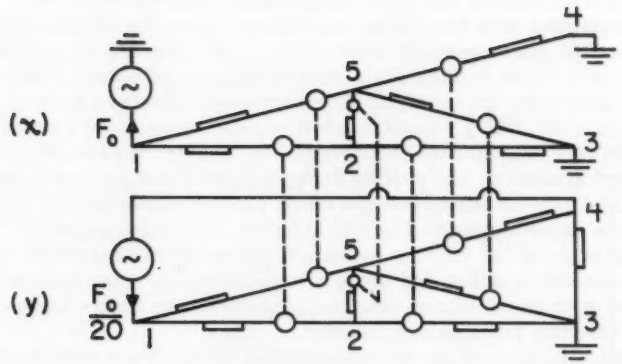

(b) analog

Fig. 5 COLUMN-LIKE TRUSS AND ANALOG

joints both capital and lower-case letters can be used, as well as foreign language characters.

2. Choose reference directions for axes x and y as well as for slope (θ), and show the loads and reactions, the latter assumed unknown. For uniformity show reaction moments in the direction of positive slope, and resolve the reaction forces in the x- and y-directions where practicable.
3. Assign a reference positive direction, and therefore a unique beginning and end, to each member. For convenience this direction may be the alphabetical direction of the joint designations; if the opposite direction is preferred as a reference in some cases, indicate this by an arrow on the member.
4. Designate the x- and y-forces acting on each member, as dictated by equilibrium considerations alone. Use the following conventions: above or to the left of the member indicate the x-force applied to the member

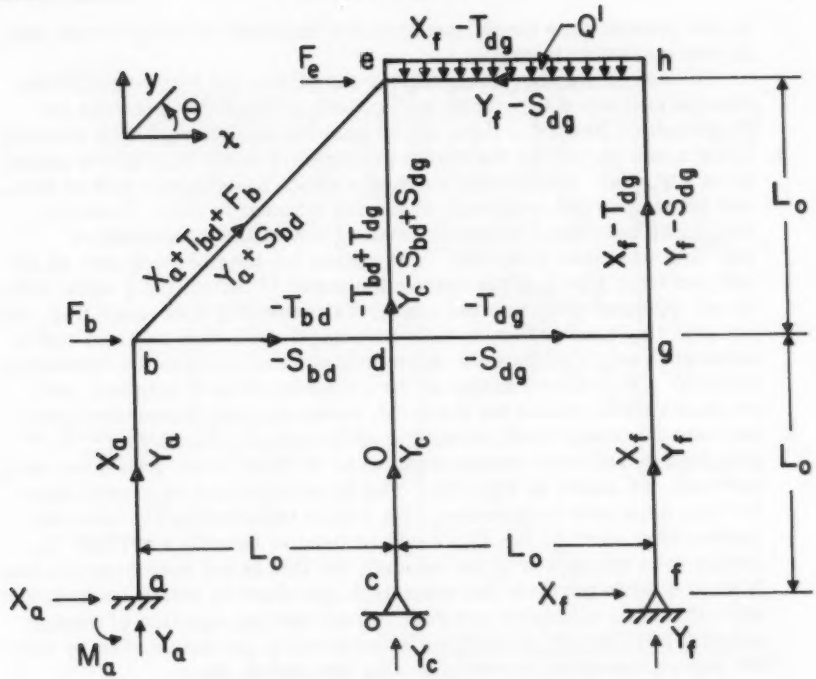

Fig. 6 RIGID FRAME

at its beginning; below or to the right of the member indicate the corresponding y-force. The result is shown in Fig. 6. Where the member forces are redundant in that they cannot be obtained by equilibrium considerations alone, express them in terms of the unknown tension T (negative if compressive) and the shear S, the latter being considered positive when it tends to rotate the member in the direction of positive slope. (For example, for a horizontal member such as d-g running from left to right, a force at the beginning of the member in the positive y-direction is the negative of shear force.) The joint-force equilibrium considerations must also satisfy the two force summations applicable to the structure as a whole, namely:

$$F_b + F_e + X_a + X_f = 0 \tag{10}$$

$$Y_{a-f} - W = 0 \tag{11}$$

where

$$Y_{a-f} \equiv Y_a + Y_c + Y_f \tag{12}$$

In the present case these equations are satisfied by the x-forces and y-forces applied to joint e.

The use of the above conventions simplifies the force-equilibrium calculations since it permits one to think of the x- or y-forces as electrical or hydraulic flows in the positive direction of each member.

5. Draw a new picture of the frame preparatory to developing the analog as in Fig. 7(a). Ground the terminals where the slope is held to zero, and leave open the terminals where the moment is zero. Draw the analogs of individual members, making use of the symbolism of Fig. 2(c) wherever possible. (The analog for member e-h may be developed from Fig. 5 of the companion paper,(1) by letting q equal infinity and qQ equal Q'; while the analog for member g-f is simplified, without affecting total power, to take advantage of the fact that one end is moment-free). Compute the appropriate shear currents by inspection of the x- and y-forces acting at the beginning of each member, and designate these values but leave the shear-current connections open.
6. Now use ingenuity freely in setting up transformers, current-generators, and inter-connections so as to develop the necessary shear currents, as shown in Fig. 7(b). The three equations of overall equilibrium must also be satisfied. Eq. (10) is satisfied by the currents approaching point Z; Eq. (11) could be used to develop a current Y_c (which does not appear in the analog), but this is not done here because it is so easy to perform the equivalent operation by direct computation after the other unknowns are determined; and the equation of overall moment equilibrium is satisfied automatically, as can be seen by taking the summation of all currents leaving the analog, thus:

$$M_a + L_o(X_a + Y_f - Y_a + Y_f - F_e - Q'/2) = 0$$

which represents the moment summation about joint d.

There are many other ways in which the shear currents can be developed. All are satisfactory if the conditions of redundancy are identical in the analog and in the structure, as discussed in connection with Fig. 4.

7. Assume a unit of length which will give a convenient value for some characteristic length L_o in the structure. Choose convenient scale factors relating electrical resistance to bending compliance, and current to moment. The scale factors between voltage and slope, and between voltage and the ratio of deflection and L_o, will then be fixed. Set the resistance within the individual moment networks to appropriate values for each member, switch on the generators, and read currents and voltages as desired.
8. Finally, to check the results of the work by an entirely independent method, determine by structural analysis whether the values of force and moment yielded by the analog are in equilibrium, and whether they result in slopes and deflections compatible with each other. In general there will be one compatibility check for each degree of redundancy. In indeterminate structures this checking procedure ordinarily requires a very small fraction of the time required for conventional analytical solution of the structure.

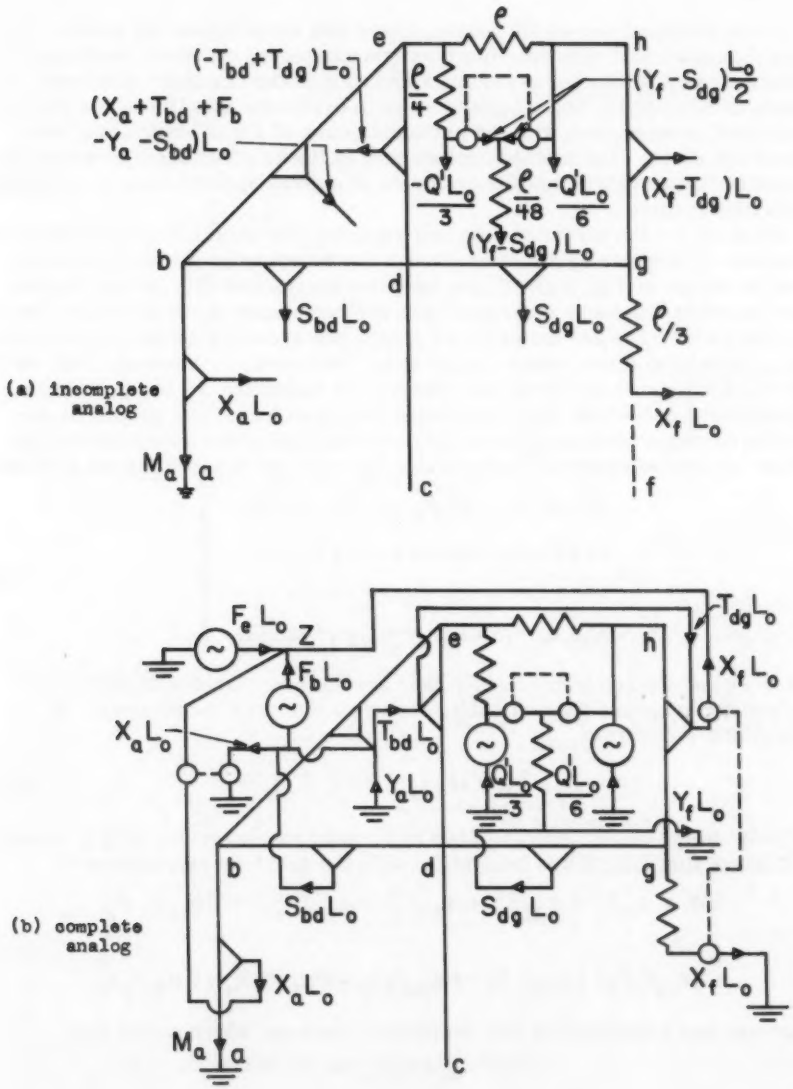

Fig. 7 ANALOG FOR Fig. 6

Partitioning of Structures

In the practical use of the analog, cases will arise where the number of available electrical elements (such as transformers, resistors, and current sources) is not sufficient to permit simulation of the complete structure. A means of simplifying the structure so as to overcome this limitation will be described in connection with the particular case of Fig. 6, which has been discussed above. The method applies only to linear structures, in which the response to successive equal increments of a given applied force or moment remains the same.

First we cut the structure into two separate sub-structures of which at least one is in static equilibrium (though not necessarily statically determinate) as shown in Fig. 8(a). At the inter-connections of this portion (in this case the right-hand sub-structure) with the remainder of the structure there are unknown forces and moments as shown, the symbol $\underline{F}$ being used to indicate generalized force, which can be either true force or moment. Now write the following equations giving the generalized deflection δ', which denotes translational deflection when associated with true force, and rotational deflection or slope when associated with moment; the prime indicates that the effects of applied external loads, in this case $\underline{Q}'$, are ignored for the present:

$$\left.\begin{aligned} \delta_1' &= a_{11}F_1 + a_{12}F_2 + a_{13}F_3 + a_{14}F_4 \\ &\cdots\cdots\cdots\cdots\cdots\cdots\cdots \\ &\cdots\cdots\cdots\cdots\cdots\cdots\cdots \\ \delta_4' &= a_{41}F_1 + a_{42}F_2 + a_{43}F_3 + a_{44}F_4 \end{aligned}\right\} \qquad (13)$$

where F_5 and F_6 are ignored since they are not associated with deflection. The constants a_{ij} are conventionally known as influence coefficients. By Castigliano's Theorem

$$\delta_i = \partial W'/\partial F_i \qquad i = 1, 2, 3, 4 \qquad (14)$$

where $\underline{W}'$ is the elastic energy of the right-hand sub-structure with $\underline{Q}'$ ignored. By trial we find that this is compatible with the previous expressions if

$$2W' = a_{11}F_1^2 + a_{22}F_2^2 + a_{33}F_3^2 + a_{44}F_4^2 + 2a_{12}F_1F_2$$
$$+ 2a_{13}F_1F_3 + 2a_{14}F_1F_4 + 2a_{23}F_2F_3 + 2a_{24}F_2F_4 + 2a_{34}F_3F_4 \qquad (15)$$

where use has been made of the reciprocity theorem, which states that

$$a_{ij} = a_{ji}$$

We next seek to reduce quadratic expression (15) to a sum of squares. Following the method of Lagrange,(6) we first write

$$2W' = \frac{1}{a_{11}}(a_{11}F_1 + a_{12}F_2 + a_{13}F_3 + a_{14}F_4)^2 + b_{22}F_2^2 + b_{33}F_3^2$$
$$+ b_{44}F_4^2 + 2b_{23}F_2F_3 + 2b_{24}F_2F_4 + 2b_{34}F_3F_4$$

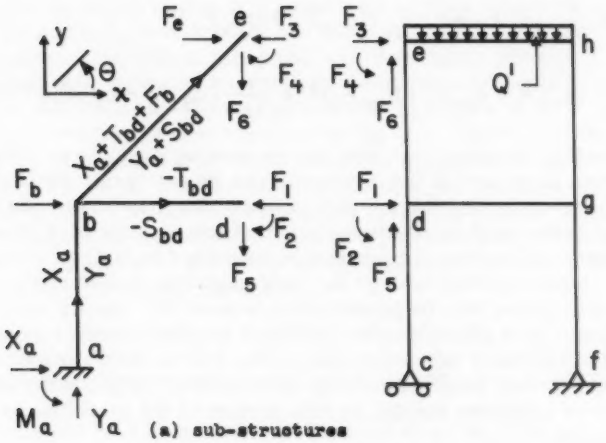

(a) sub-structures

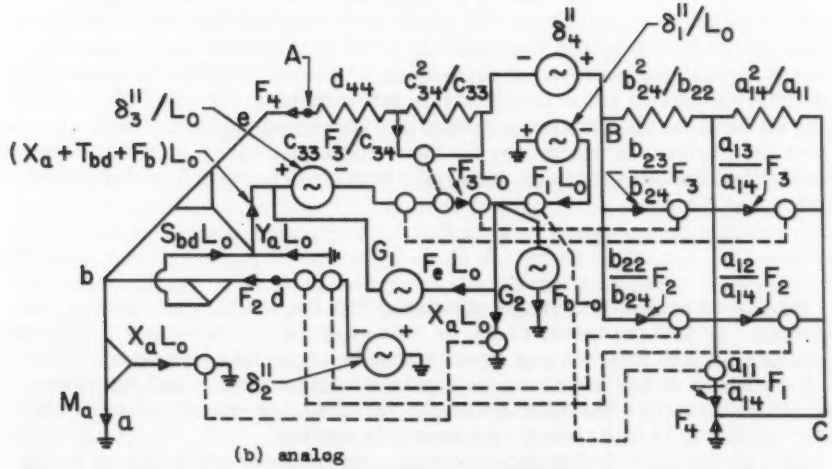

(b) analog

Fig. 8 ANALOG OF PARTITIONED STRUCTURE

where the b's depend on certain of the a's, and F_1 appears only in the first term on the right. Continuing this technique in successive steps we finally have:

$$2W' = \frac{1}{a_{11}}(a_{11}F_1 + a_{12}F_2 + a_{13}F_3 + a_{14}F_4)^2$$

$$+ \frac{1}{b_{22}}(b_{22}F_2 + b_{23}F_3 + b_{24}F_4)^2 + \frac{1}{c_{33}}(c_{33}F_3 + c_{34}F_4)^2 + d_{44}F_4^2 \quad (16)$$

By inspection we determine that it is in general possible to choose values for the forces such that all but any one of the square terms equal zero. Since the elastic energy is positive for any values of the forces, the coefficient of each square term must be positive, so that it can be simulated by an electrical resistance. If each quantity within parentheses is further simulated by electrical current flowing through the corresponding resistor, then the resulting power dissipation will be proportional to twice the elastic energy of the sub-structure. If in addition these resistors are connected to an analog which simulates the left-hand sub-structure in Fig. 8(a) in such a manner as to simulate equilibrium requirements by current-continuity considerations, the analogy will be complete insofar as this portion of the structure is concerned, with $\underline{Q}'$ ignored.(7)

To take the latter into account we must withdraw from the analog an amount of power equal to twice the work, $\underline{W}''$, which is imposed on the right-hand sub-structure by the displacement of the generalized inter-connection forces through the generalized deflections δ'' caused by $\underline{Q}'$ (or in general, by all external applied loads acting on this sub-structure). To find $\underline{W}''$, imagine that all external loads on the structure are increased uniformly from zero to their final values, in which case the inter-connection forces and their associated deflections also increase uniformly from zero to their final values, so that

$$2W'' = \sum_{i=1}^{4} F_i \, \delta_i'' \qquad i = 1, 2, 3, 4 \quad (17)$$

As will be shown, this can be simulated with the aid of fixed voltage sources. To find the values of δ_i'', as well as of the constants in Eq. (13) and consequently Eq. (16), we may assume that the right-hand sub-structure in Fig. 8(a) is an actual structure, set up its electrical analog, and determine the inter-connection deflections with the various inter-connection forces and external loads (in this case $\underline{Q}'$) successively applied.

As a preliminary to drawing the analog, we denote $\underline{x}$- and $\underline{y}$-forces acting at the beginning of various members of the left-hand sub-structure in the same manner as was done in Fig. (6), and then express the inter-connection forces in terms of other forces and moments by considering equilibrium at joints $\underline{d}$ and $\underline{e}$, thus:

$$F_1 = -T_{db} \qquad F_2 = -M_{db}$$

$$F_3 = X_a + T_{db} + F_b + F_e \qquad F_4 = -M_{eb}$$

$$F_5 = -S_{bd} \qquad F_6 = Y_a + S_{bd}$$

As to considerations of overall equilibrium, moment equilibrium will presumably be automatically satisfied by the analog as before, while force equilibrium yields no additional information over what we already have.

The analog is shown in Fig. 8(b), where the portion representing the left-hand sub-structure is developed by the same method as before. The currents F_2 and F_4 appear directly in this portion of the analog, while F_3L_o and F_1L_o are developed with the aid of current generators G_1 and G_2 in accordance with the above equations. Power equal to $2\underline{W}'$ is simulated by means of transformers and resistors in accordance with Eq. (16), where however the coefficients of F_4 have been factored out wherever F_4 appears between parentheses; this saves several transformers by avoiding the need for multiplying F_4 by various values. The power represented by Eq. (17) is simulated with the aid of voltage generators of suitable polarity, as indicated, to absorb power since $\underline{W}''$ represents work absorbed by the right-hand sub-structure. The sum of all currents leaving the analog is:

$$M_a - F_2 - F_4 + L_o(2X_a - Y_a + F_b - F_1) = 0$$

which represents the moment summation of the left-hand sub-structure about joint e.

In the present case it is clear that there is no great saving in circuit components resulting from the use of the partitioning technique. Obviously this method increases in usefulness as the number of members in the first sub-structure increases and the number of inter-connection forces between both sub-structures decreases.

Applied Deflections and Thermal Effects

In addition to applied forces and moments, structures are often subjected to applied deflections and slopes, as when a joint of the structure is displaced or rotated by a prescribed amount. This is closely associated with thermal effects, which change the (unloaded) shape of a member, so that stresses result if the change of shape is restricted by adjacent members. This phenomenon is important in piping systems carrying fluid at varying temperatures.

A general method for modifying the analog so as to deal with applied changes of shape, whether resulting from thermal effects or not, is given in the following rules. Like the rules relating to the remainder of the analog, these employ current-continuity and energy concepts alone, and their validity is easily proved by the energy theorems previously stated, plus the reasoning associated with Eq. (17).

1. Select a force (or moment) $\underline{F}'$ which would result in the deflection (or slope) δ' of interest, and arrange the analog so as to simulate $\underline{F}'$ by a current proportional to it.
2. In series with this current insert a voltage generator, of voltage proportional to δ', the constant of proportionality being such that the power supplied to the analog by the generator equals $F'\delta'$.

As an example, suppose that joint 1 in Fig. 1 is given a known deflection δ' in the y-direction, or alternatively that member 1-2 alone is heated to such a temperature that its free expansion would be δ'. The structural effect is the same in either case, the associated force being Y_1. To simulate this it is

merely necessary to insert at point S in Fig. 4, where the current $Y_1 L_O$ flows, a voltage difference δ'/L_O, with polarity such that the voltage rises in the downward direction so that the power $Y_1 \delta'$ is supplied to the circuit. All currents and voltages in the analog then automatically adjust themselves to new values consistent with the value of δ'.

Experimental Work

A new model of the equipment has been built and is shown in Fig. 9. It need not be described in detail because it is essentially the same as the equipment shown in Fig. 11 of the companion paper.(1) However, the general layout and certain details have been modified to permit more convenient operation than in the previous case, and space has been conserved and accuracy increased by omitting the resistor knobs and dials and instead providing for precise screw-driver setting of the resistors using a built-in Wheatstone bridge arrangement.

Transformer Imperfections

The present equipment incorporates a 400-cycle power supply, which yields smaller errors due to transformer imperfections than the 60-cycle supply previously used. Further, a quadrature-rejection circuit of a type conventionally known to electrical engineers is incorporated in series with the panel meter, which, as before, acts as a galvanometer in combination with the adjacent 10-turn potentiometer to measure voltage by a conventional nulling technique; this circuit renders the meter insensitive to phase shift, which is the principal effect of the series and shunt inductances of the transformers, and which tends to cause a broad null.

The series resistances of the transformer windings can often be absorbed within analog resistances to which they happen to be connected. Sometimes, however, such contiguous resistances do not exist in the analog, so that it may be desirable to compensate for the winding resistances, as well as for the effective shunt resistance of each transformer, which in general cannot be absorbed within analog resistances. This can be effected with the aid of power admitted to the transformer through a compensating winding, which may or may not be part of the primary or secondary; however, no such compensation was found necessary.

Where more than one transformer carries a current proportional to a single force or moment, their combined winding resistances may be referred to a single winding in such a way that the total power is unaffected. Alternatively, the voltage drop across a winding resistance may be negated by a suitable applied voltage drop.

Error Criteria

In the following experimental work each of the force errors in a given structure is expressed not as a percentage of its own theoretical value, but rather as a percentage of a single reference force selected as the largest or the most significant in the structure. The reason for this choice of error criterion is that, because of practical imperfections both in the analog and in the actual structure, the various forces in the analog and in the structure tend to differ from their theoretical values by absolute values which are of the same

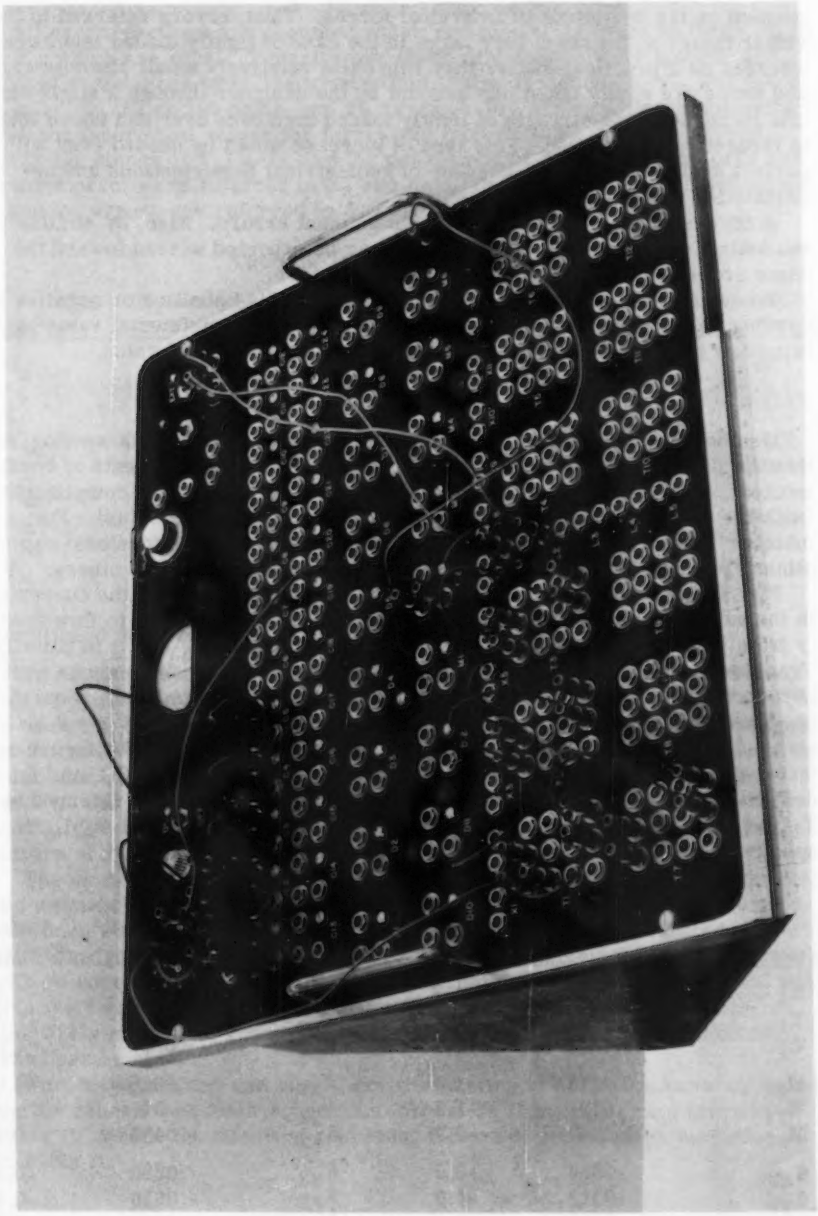

order of magnitude throughout the structure, and which are not highly dependent on the magnitude of individual forces. Thus, errors referred to individual values might seem very large in the case of lightly loaded members, whereas as a practical matter they represent relatively small absolute errors and hence are easily taken into account by the designer through a slight absolute increase in the strength of lightly loaded members over and above what is theoretically required. This type of increase would be needed even with a perfect analytical solution, because of geometrical imperfections and uncertainties of loading of the structure.

A corresponding argument holds for moment errors. Also, by similar reasoning, deflection and slope errors may be expected to tend toward the same order of magnitude throughout the structure.

To avoid confusion due to signs, an error is called positive or negative according as the absolute magnitude of the associated experimental value is larger or smaller than that of the corresponding theoretical value.

Frame of Figs. 1, 3, 4

Members 1-2 and 2-3 were assumed to have a circular cross-section, so that the flexural moment of inertia I is constant for all components of bending moment, and the torsional compliance is 5/4 times the bending compliance (with the shear modulus assumed equal to 2/5 of Young's modulus). For member 3-4 the values of I were assumed the same, but the torsional compliance per unit length was considered twice as great as for the others.

Fig. 4 was modified by multiplying the voltages and dividing the currents in the sub-network ABCD by $\sqrt{2}$, thus permitting current X_1L_o to flow directly from point O to point E, and current M_{y34} from points F and G to point H. Transformer shunt resistances were ignored, and winding resistances were absorbed within analog resistances except for transformers handling currents M_{y34} and M_{z34}. L_o was taken as unity, L_o/EI as 100 ohms, and $\sqrt{2}$ F as about .05 ampere. In the following table the theoretical values for forces are factors of $\sqrt{2}$ F, for moments of $\sqrt{2}FL_o$, for slopes of $\sqrt{2}FL_o^2/EI$, and for deflections of $\sqrt{2}FL_o^3/EI$. The errors in force and moment are referred to X_1 and X_1L_o respectively, and in slope and deflection to θ_{z2} and $\theta_{z2}L_o$ respectively.

Table I. Frame of Figs. 1, 3, 4

Unknown	Theoretical Value	Analog Error, %	Unknown	Theoretical Value	Analog Error, %
X_1	-0.4884	-1.3	θ_{x3}	-.0755	-1.4
Y_1	-0.2333	-0.7	θ_{y3}	-.0154	+1.3
Z_1	-0.1074	-0.1	θ_{z3}	-.0534	-1.9
M_{x1}	-0.1171	+1.3	δ_{x2}	.0860	+0.1
M_{y1}	- .0170	-1.0	δ_{y2}	0	---
M_{z1}	0.3347	-0.7	δ_{z2}	-.0406	-0.2
θ_{x2}	- .0634	-0.9	δ_{x3}	.0860	+0.1
θ_{y2}	.0213	-1.0	δ_{y3}	-.0526	-0.8
θ_{z2}	- .0905	-0.4	δ_{z3}	-.0526	-0.8

Frame of Figs. 6, 7

All cross-sections are assumed equal, and load Q' is twice as large as F_b or F_e, which are equal. Transformer shunt resistances were ignored and winding resistances were absorbed within analog resistances. L_o was taken as unity, L_o/EI as 100 ohms, and F_b as about .025 ampere. In the following table the theoretical values for forces are factors of F_b, for moments of F_bL_o, for slopes of $F_bL_o^2/EI$, and for deflections of $F_bL_o^3/EI$. The force and moment errors are referred to X_a and X_aL_o respectively, and the deflection and slope errors are referred to δ_{xb} and δ_{xb}/L_o respectively.

Table II. Frame of Figs. 6, 7

Unknown	Theoretical Value	Analog Error, %	Unknown	Theoretical Value	Analog Error, %
M_a	0.9216	-0.8	T_{dg}	-0.5207	+0.7
X_a	-1.6248	-1.5	Y_f	1.0436	+2.1
X_f	-0.3752	-0.8	θ_b	-0.1092	+0.9
M_{bd}	-0.3739	-0.3	θ_d	.0314	-1.7
S_{bd}	0.4666	-0.5	θ_g	- .0650	+0.9
M_{dg}	- .0041	+1.1	θ_e	- .0144	+1.0
S_{dg}	0.2010	+2.0	θ_h	.0406	-1.9
T_{bd}	-0.4188	+1.2	δ_{xb}	0.1900	+1.3
Y_a	-2.0348	+0.2	δ_{xe}	0.1900	+1.3

Partitioned Frame of Figs. 6, 8

To obtain a good test for the validity of Fig. 8(b) it was considered advisable to determine the values of the influence coefficients in Eqs. (14) and (16) by analysis, rather than by the application of the analog to the right-hand substructure in Fig. 8(a) as would be done in practice. Table III shows pertinent values including those of use in constructing Fig. 8(b). With L_o assumed equal to unity, the numbers given for influence coefficients are factors of L_o/EI. The table also shows values of δ'', with the numbers representing factors of $F_bL_o^3/EI$.

The scale factors between compliance and resistance and between current and moment were the same as in the previous case. Transformer shunt resistances were ignored, and winding resistances were compensated either by being absorbed within analog resistances or by suitable adjustment of the voltage sources simulating δ''. Since the resistors in sub-network ABC were relatively very low, the voltage and currents in this sub-network were respectively multiplied and divided by 10 by means of a suitable connected transformer at point A.

Theoretical values and analog errors relating to certain unknowns, including the generalized inter-connection forces F_1 through F_4, are given in Table III, where the numbers represent factors of appropriate quantities as in Table II.

CONCLUSIONS

The analog can yield relatively rapid solutions for a wide variety of linear and non-linear framed structures, including 3-dimensional rigid frames. It

Table III. Partitioned Frame of Figs. 6, 8

Values Needed for Setting Up Analog

a_{11}	0.5000	a_{34}	-0.0833	a_{14}^2/a_{11}	0.0035
a_{12}	0.0208	a_{44}	0.1667	b_{24}^2/b_{22}	0.0022
a_{13}	0.5417	a_{11}/a_{14}	-12.0000	c_{34}^2/c_{33}	0.0272
a_{14}	-0.0417	a_{12}/a_{14}	-0.5000	δ_1''	0.0104
a_{22}	0.1667	a_{13}/a_{14}	-13.0000	δ_2''	0.0104
a_{23}	-0.0208	b_{22}/b_{24}	8.6818	δ_3''	0.0104
a_{24}	-0.0208	b_{23}/b_{24}	2.2727	δ_4''	-0.0312
a_{33}	0.6667	c_{33}/c_{34}	-1.5858		

Unknowns	Theoretical Value	Analog Error, %	Unknowns	Theoretical Value	Analog Error, %
M_a	0.9216	+1.2	F_3	- .0436	-1.0
X_a	-1.6248	-1.2	F_4	0.1953	+0.4
M_{bd}	-0.3739	+0.2	θ_b	-0.1092	-0.2
S_{bd}	0.4666	-0.2	θ_d	.0314	+0.0
F_1	0.4188	+0.2	θ_e	- .0144	-0.2
F_2	.0927	-0.1	δ_{xb}	0.1900	-0.0

is usually unnecessary to derive the governing equations (as is generally required with general-purpose analog computers), and it is particularly easy to explore the effects of modifying the dimensions of structural members, which is useful in design procedures. The use of energy theorems make it possible to obtain slopes and deflections without considering them explicitly in setting up the analog circuitry, resulting in relative simplicity and in economy of analog elements.

The relative ease of conducting a separate check makes it feasible to detect gross errors due to misuse or defects of the analog.

The accuracy is in general consistent with the accuracy of assumptions relating to such things as conditions of end fixity, dimensions of members, joint conditions, and the neglect of direct shear and tensile effects in bending members. The error may become significant in special cases, such as in shallow trusses subjected to high longitudinal compressive load, where the transformer voltage drops are very large compared to the voltage drops across analog resistances.

Techniques have been included for dealing with applied deflections and thermal effects, and for partitioning structures which have too many members for simultaneous simulation on an analog instrument.

Appendix. Notation

a	influence coefficient;
A	cross-sectional area;
b, c, d	modified influence coefficients;
E	Young's modulus
F	force; generalized force (including moment); currents analogous to same;
F'	force associated with applied deflection; current analogous to same;
G	shear modulus;
I	moment of inertia effective in bending;
I_T	moment of inertia effective in torsion;
L	length;
M	moment; current analogous to moment;
Q'	distributed load; current analogous to distributed load;
S	shear force;
T	tensile force; current analogous to tensile force;
u, v	rectangular coordinates;
x, y, z	rectangular coordinates;
X, Y, Z	force in the respective coordinate directions;
δ	deflection; voltage analogous to deflection;
δ'	generalized deflection (including slope); applied deflection; voltage analogous to same;
δ''	generalized deflection caused by external applied loads; voltage analogous to same;
θ	elastic slope; voltage analogous to elastic slope; and
ρ	resistance analogous to bending compliance.

REFERENCES

1. "Electrical Analogs of Statically Loaded Structures", by F. L. Ryder, Transactions ASCE, Vol. 119, 1954, p. 1046.
2. See for example "The Direct Analogy Analog Computer," by G. D. McCann, ISA Journal, April 1956 which contains an extensive bibliography.
3. "Network Analysis by Least Power Theorems," by F. L. Ryder, Journal of The Franklin Institute, Vol. 254, July, 1952, p. 47.
4. "The Analysis of Linear and Non-Linear Framed Structures," by F. L. Ryder, Doctorate Thesis filed in Library of New York University, December, 1950.

5. A treatment of this is given in "Strength of Materials, Part II," by S. Timoshenko, D. Van Nostrand Co., New York, 1941, p. 371.

6. See "Introduction to Higher Algebra", by M. Bocher, the MacMillan Co., New York, 1907, p. 131.

7. Similar results may be obtained by dealing with Eqs. (13) in a manner described by Cauer in "Ideal Transformers and Linear Transformations," Elektrische Nachrichten Technik, Vol. 9, p. 154, May 1932; however, the present method is more appropriate here in that it is based on energy considerations in place of the compatibility considerations used by Cauer, as a consequence of which the transformer voltage drops need not be considered explicitly.

Journal of the
ENGINEERING MECHANICS DIVISION
Proceedings of the American Society of Civil Engineers

ON LONGITUDINAL WAVES IN AN ELASTIC PLATE[a]

E. Volterra,[1] M. ASCE and E. C. Zachmanoglou[2]

ABSTRACT

The problem of dispersion of longitudinal waves in an elastic infinite plate is discussed by applying the Method of Internal Constraints and by taking into account second order terms in the equations of constraints. Numerical results obtained by applying this theory are compared with those obtained by applying the exact theory given by Lamb.

NOMENCLATURE

The following nomenclature is used in the text:

x, y, z = rectangular coordinates

u, v, w = components of the elastic displacement in the x, y, z axes

t = time

$\epsilon_x, \epsilon_y, \epsilon_z, \gamma_{xy}, \gamma_{xz}, \gamma_{yz}$ = components of strain

h = thickness of the plate

U = potential energy of the plate

T = kinetic energy of the plate

Note: Discussion open until June 1, 1959. To extend the closing date one month, a written request must be filed with the Executive Secretary, ASCE. Paper 1896 is part of the copyrighted Journal of the Engineering Mechanics Division, Proceedings of the American Society of Civil Engineers, Vol. 85, No. EM 1, January, 1959.

a. The results presented in the paper were obtained in the course of an investigation sponsored by the Office of Ordnance Research and by the National Science Foundation.

1. Prof. and Chmn., Eng. Mechanics Dept., Univ. of Texas, Austin, Tex.
2. I.B.M. Fellow, Univ. of California, Berkeley, Calif.

E = Young's modulus)
σ = Poisson's ratio)
ρ = density)
$G = \frac{E}{2(1+\sigma)}$) for the material of the plate
$\lambda = \frac{E}{(1+\sigma)(1-2\sigma)}$)
L = wave length
c = wave velocity
$\alpha = \frac{\sigma}{1-\sigma}$
$\beta = \frac{8}{15}\frac{1-\sigma}{(1+\sigma)(1-2\sigma)}$
$\gamma = \frac{2\pi}{L}$
$\delta = \frac{4}{3}\frac{1}{2(1+\sigma)}$

INTRODUCTION

The problem of two-dimensional waves in a solid bounded by parallel planes has been considered by Lord Rayleigh[1] and by Professor H. Lamb[2] in two well-known papers published respectively in the years 1888 and 1917. Recently, J. P. Marsden[3] numerically computed dispersion curves for longitudinal waves from the theory given by Lamb. The object of this paper is to discuss the problem of dispersion of longitudinal waves in an infinite elastic plate (plane strain problem) by applying the Method of Internal Constraints, and to compare the numerical results obtained by this theory with those computed by Marsden using Lamb's theory.*

The present paper complements two previous papers,[4,5] in which the problem of dispersion of longitudinal waves in elastic straight rods of infinite lengths and of rectangular and circular cross sections were discussed by applying a one-dimensional approximate theory of wave propagation based on the Method of Internal Constraints. It was the late Professor R. M. Davies who advised the authors to compare the results given by the approximate theory with those given by the exact theory by checking the magnitudes of the field vectors and their variations over the cross-section.[6]

The infinite plate of constant thickness h will be referred to a system of orthogonal cartesian coordinates x, y, z, the xz plane coinciding with the middle surface of the plate (see Fig. 1). The motion is supposed to take place in two dimensions xy.

*The authors are indebted to the late Professor R. M. Davies, former Head of the Department of Physics at the University College of Wales in Aberystwyth, for having furnished them with numerical data which have been used for comparison in some of the figures enclosed in the text.

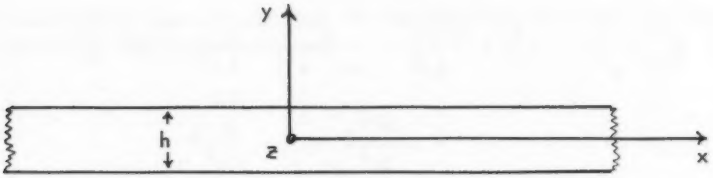

FIGURE 1

Calling u, v, w the components of the elastic displacement in the x, y, z directions, let

$$\left.\begin{aligned} u(x, y;t) &= v_x(x, t) + \left(\frac{y}{\frac{h}{2}}\right)^2 f_x(x, t) \\ v(x, y;t) &= y\,\lambda_y(x, t) + \left(\frac{y}{\frac{h}{2}}\right)^3 f_y(x, t) \\ w(x, y;t) &= 0 \end{aligned}\right\} \qquad (1)$$

The condition that on the free surfaces of the plate ($y = \pm \frac{h}{2}$) the normal stress σ_y should vanish is expressed by the following equation

$$(\sigma_y)_{y=\pm\frac{h}{2}} = (\lambda + 2G)\left[\lambda_y + 3f_y + \alpha\left(\frac{\partial v_x}{\partial x} + \frac{\partial f_x}{\partial x}\right)\right] = 0 \qquad (2)$$

where

$$\alpha = \frac{\sigma}{1 - \sigma}$$

$$\lambda = \frac{\sigma E}{(1 + \sigma)(1 - 2\sigma)}$$

$$G = \frac{E}{2(1 + \sigma)}$$

E being Young's modulus and σ Poisson's ratio of the material of the bar. From Eq. (2), it follows:

$$f_y = -\frac{1}{3}\left[\lambda_y + \alpha\left(\frac{\partial v_x}{\partial x} + \frac{\partial f_x}{\partial x}\right)\right] \qquad (3)$$

Substituting Eq. (3) into Eqs. (1), the components of the elastic displacement will be expressed by the following relationships:

$$\left.\begin{aligned} u &= v_x + \left(\frac{y}{\frac{h}{2}}\right)^2 f_x \\ v &= y\,\lambda_y - \frac{1}{3}\left[\left(\frac{y}{\frac{h}{2}}\right)^2 \lambda_y + \alpha\left(\frac{\partial v_x}{\partial x} + \frac{\partial f_x}{\partial x}\right)\right] \end{aligned}\right\} \qquad (1')$$

On the assumptions that no external forces (body and surface forces) are applied to the infinite plate and that the plate has constant thickness h, the following equations of motion are obtained (see Appendix to the paper).

$$
\left.
\begin{aligned}
&E\left(\frac{1}{1-\sigma^2}+\alpha^2\beta\right)\frac{\partial^2 v_x}{\partial x^2}+\frac{E}{3(1-\sigma^2)}\frac{\partial^2 f_x}{\partial x^2}+E\alpha\beta\frac{\partial \lambda_y}{\partial x}=\\
&\qquad=\rho\frac{\delta^2 v_x}{\delta t^2}+\frac{1}{3}\rho\frac{\delta^2 f_x}{\delta t^2}\\
&\frac{E}{5(1-\sigma^2)}\left(\frac{h}{2}\right)^2\frac{\delta^2 f_x}{\partial x^2}+\frac{E}{3(1-\sigma^2)}\left(\frac{h}{2}\right)^2\frac{\delta^2 v_x}{\partial x^2}-E\,\delta f_x-\\
&-E\varepsilon\left(\frac{h}{2}\right)^2\frac{\partial \lambda_y}{\partial x}=\frac{\rho}{5}\frac{\partial^2 f_x}{\partial t^2}+\frac{\rho}{3}\frac{\partial^2 v_x}{\partial t^2}\\
&\frac{E}{3}\,\frac{1+\frac{K^2}{2L}-\frac{2K}{5}}{2(1+\sigma)}\left(\frac{h}{2}\right)^2\frac{\partial^2\lambda_y}{\partial x^2}-E\,y+E\varepsilon\frac{\partial f_x}{\partial x}-\\
&-E\alpha\beta\frac{\partial v_x}{\partial x}=\frac{\rho}{3}\left(1+\frac{K^2}{2L}-\frac{2K}{5}\right)\left(\frac{h}{2}\right)^2\frac{\partial^2\lambda_y}{\partial t^2}
\end{aligned}
\right\} \qquad (4)
$$

where

$$\beta = \frac{8}{15}\,\frac{1-\sigma}{(1+\sigma)(1-2\sigma)}$$

$$\delta = \frac{4}{3}\,\frac{1}{2(1+\sigma)}$$

$$\varepsilon = \frac{2}{3}\,\frac{1-\frac{K}{5}}{2(1+\sigma)}$$

The factor K which appears in Eqs. (4) is defined as

$$K = 1+\alpha\,\frac{\frac{\partial v_x}{\partial x}+\frac{\partial f_x}{\partial x}}{\lambda_y} \qquad (5)$$

The Velocity Equation

Let:

$$
\left.
\begin{aligned}
v_x &= A_1 e^{i\gamma(x-ct)}\\
f_x &= A_2 e^{i\gamma(x-ct)}\\
\lambda_y &= A_3 e^{i\gamma(x-ct)}
\end{aligned}
\right\} \qquad (6)
$$

Where A_1, A_2, A_3 are constants, C the phase velocity, $\gamma = \frac{2\pi}{L}$ the wave number, L the wave length and $i = \sqrt{-1}$.

By substituting Eqs. (6) into Eqs. (4), the following three homogeneous equations in A_1, A_2, A_3 are obtained

$$\begin{aligned}
&Z_1 A_1 + \frac{Z_2}{3} A_2 + \alpha\beta \frac{i}{\gamma} A_3 = 0 \\
&\gamma^2 \left(\frac{h}{2}\right)^2 \frac{Z_2}{3} A_1 + \left[\gamma^2 \left(\frac{h}{2}\right)^2 \frac{Z_2}{5} - \delta\right] A_2 - \gamma^2 \left(\frac{h}{2}\right)^2 \varepsilon \frac{i}{\gamma} A_3 = 0 \\
&\alpha\beta A_1 - \varepsilon A_2 + \left[\gamma^2 \left(\frac{h}{2}\right)^2 Z_3 - \beta\right] \frac{i}{\gamma} A_3 = 0
\end{aligned} \tag{7}$$

where

$$Z_1 = \left[\left(\frac{c}{co}\right)^2 - \left(\frac{1}{1-\sigma^2} + \alpha^2\beta\right)\right]$$

$$Z_2 = \left[\left(\frac{c}{co}\right)^2 - \frac{1}{1-\sigma^2}\right]$$

$$Z_3 = \frac{1}{3}\left(1 + \frac{K^2}{21} - \frac{2K}{5}\right)\left[\left(\frac{c}{co}\right)^2 - \frac{1}{2(1+\sigma)}\right]$$

$$co = \sqrt{\frac{E}{\rho}}$$

By expressing that the determinant of the coefficient of Eqs. (7) is zero, the following velocity equation is obtained

$$\left(\frac{h}{L}\right)^4 A + \left(\frac{h}{L}\right)^2 B + C = 0 \tag{9}$$

where

$$\begin{aligned}
A &= \pi^4 Z_2 Z_3 \left[\frac{Z_1}{5} - \frac{Z_2}{9}\right] \\
B &= \pi^2 \left[-\beta Z_2 \left(\frac{Z_1}{5} - \frac{Z_2}{9}\right) - 2\alpha\beta\varepsilon \frac{Z_2}{3} - (\varepsilon^2 + \delta Z_3) Z_1 - \alpha^2\beta^2 \frac{Z_2}{5}\right] \\
C &= \beta\delta \left[Z_1 + \alpha^2\beta\right] = \beta\delta \left[\left(\frac{c}{co}\right)^2 - \frac{1}{1-\sigma^2}\right]
\end{aligned} \tag{10}$$

From Eqs. (4), the ratios $\frac{A_2}{A_1}$ and $\frac{iA_3}{\gamma A_1}$ are determined as follows:

$$\left(\frac{A_2}{A_1}\right) = -\frac{\pi^2 \left(\frac{h}{L}\right)^2 \left[\varepsilon Z_1 + \frac{\alpha\beta}{3} Z_2\right]}{\pi^2 \left(\frac{h}{L}\right)^2 Z_2 \left[\frac{\alpha\beta}{5} + \frac{\varepsilon}{3}\right] - \alpha\beta\delta}$$

$$\left(\frac{iA_3}{\gamma A_1}\right) = -\frac{\pi^2 \left(\frac{h}{L}\right)^2 Z_2 \left[\frac{Z_1}{5} - \frac{Z_2}{9}\right] - \delta Z_1}{\pi^2 \left(\frac{h}{L}\right)^2 Z_2 \left[\frac{\alpha\beta}{5} + \frac{c}{3}\right] - \alpha\beta\delta} \tag{11}$$

It should be pointed out that in order to determine the above ratios for a particular value of $(\frac{c}{co})$ the corresponding value of $\frac{h}{L}$ obtained from Eq. (9) should be used. Expressing the factor K given by Eq. (5) in terms of Eqs. (11), one gets

$$K = 1 - \alpha \frac{1 + (\frac{A_2}{A_1})}{(\frac{iA_3}{\gamma A_1})} \qquad (12)$$

As a first approximation for K, the value $K = K_1 = 1$ was assumed. For this value of K, the root of Eq. (9) for $(\frac{c}{co}) \leq \frac{1}{1 - \sigma}$ was computed using the

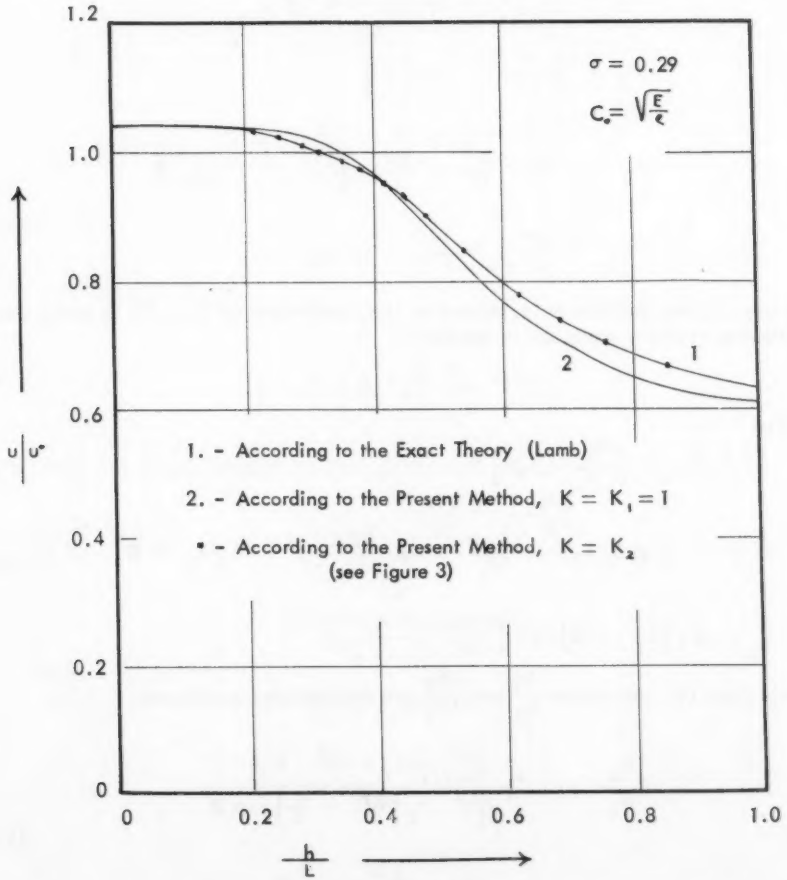

FIGURE 2

Phase velocity of longitudinal waves in plane strain

value $\sigma > 0.29$. This has been plotted in Fig. 2 and has been compared with the exact theory given by Lamb[2] and computed by Marsden.[3]

This root becomes complex for a value of c close to the value of the velocity of the Rayleigh surface waves. Apparently, the reasons for this are: first, the parabolic distortion of the cross section assumed by Eqs. (1) is not valid for short wave lengths, and second, the influence of the shear stress on the free surface of the plate, which according to the theory developed in this paper, does not vanish.

The ratios $\frac{A_2}{A}$ and $\frac{iA_3}{\gamma A_1}$ have been later computed for $K = K_1 = 1$. Using, in this case Eq. (12), a closer approximate value for the factor K has been obtained which has been designated as K_2. The variation of K_2 with $\frac{c}{co}$ is shown in Fig. 3.

The root of Eq. (9) for $\frac{c}{co} \leq \frac{1}{1 - \sigma^2}$ has been computed again for $K = K_2$. The corresponding numerical values so obtained are plotted in Fig. 2. The agreement with the exact theory given by Lamb seems to be excellent. Also in this case, however, this root becomes complex for values of c close to the values of the velocity of Rayleigh surface waves.

Components of Elastic Displacement and Stresses Along the Cross Section of the Plate

Substituting Eqs. (6) into Eqs. (1'), the following expressions are obtained for the components of the elastic displacement:

$$\left.\begin{aligned} u &= iA\left[1 + \left(\frac{y}{\frac{h}{2}}\right)^2 \left(\frac{A_2}{A_1}\right)\right] e^{i\gamma(x - ct)} \\ v &= A\left(\frac{iA_3}{\gamma A_1}\right)\pi\left(\frac{h}{L}\right)\left(\frac{y}{\frac{h}{2}}\right)\left\{1 - \frac{1}{3}\left(\frac{y}{\frac{h}{2}}\right)^2\left[1 - \alpha\frac{1 + \left(\frac{A_2}{A_1}\right)}{\left(\frac{iA_3}{\gamma A_1}\right)}\right]\right\} e^{i\gamma(x-ct)} \\ w &= 0 \end{aligned}\right\} \quad (13)$$

From Eqs. (13), the following expressions are obtained for the stresses σ_x and σ_y:

$$\frac{\sigma_x}{(\lambda + 2G)} = -A\gamma\left\{1 - \alpha\left(\frac{iA_3}{\gamma A_1}\right) + \left(\frac{y}{\frac{h}{2}}\right)^2\left[\left(\frac{A_2}{A_1}\right) + \alpha\left(\frac{iA_3}{\gamma A_1}\right)\left(1 - \alpha\frac{1 + \left(\frac{A_2}{A_1}\right)}{\left(\frac{iA_3}{\gamma A_1}\right)}\right)\right]\right\} e^{i\gamma(x-ct)} \quad (14)$$

$$\frac{\sigma_y}{(\lambda + 2G)} = A\gamma\left[\left(\frac{iA_3}{\gamma A_1}\right) - \alpha\right]\left[1 - \left(\frac{y}{\frac{h}{2}}\right)^2\right] e^{i\gamma(x-ct)}$$

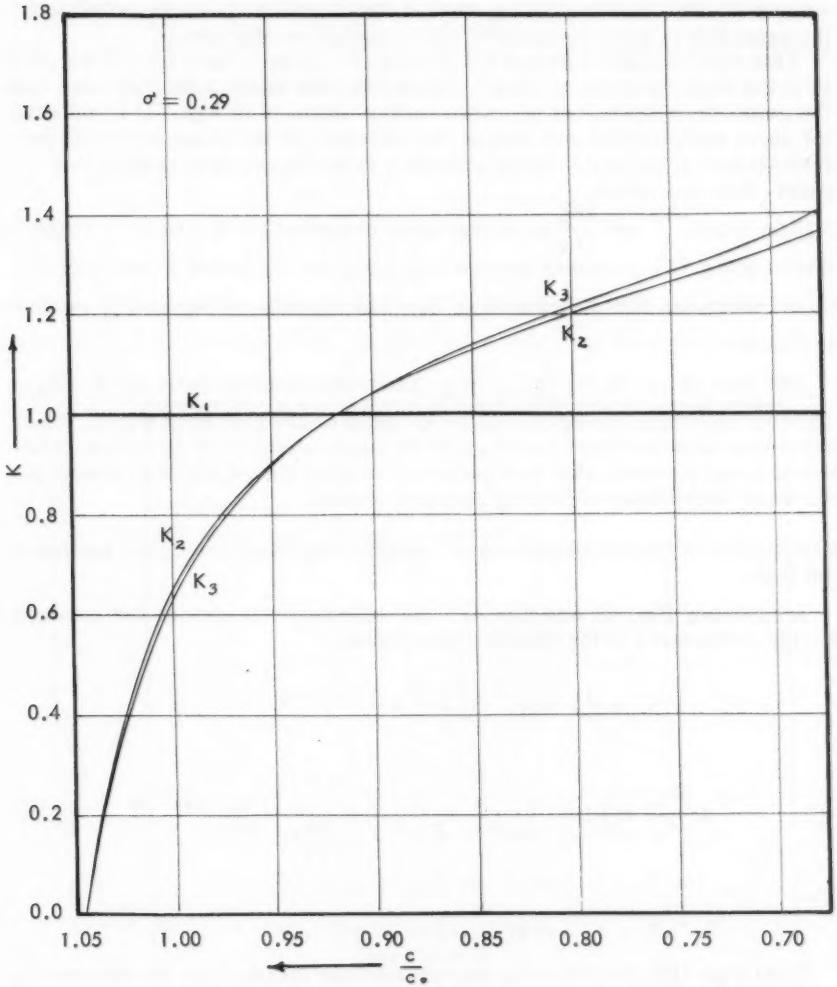

FIGURE 3

Correction factor K as a function of $\frac{c}{c_0}$

In Eqs. (13) and (14) $A = iA_1$.

The longitudinal displacement u and the longitudinal stress σ_x are in correspondence with the middle surface ($y = 0$) given by the following expressions:

$$\left.\begin{aligned} u(o) &= iAe^{i\gamma(x-ct)} \\ \frac{\sigma_x(o)}{(\lambda+2G)} &= -A\gamma\left[1-\alpha\left(\frac{iA_3}{\gamma A_1}\right)\right]e^{i\gamma(x-ct)} \end{aligned}\right\} \qquad (15)$$

In Fig. 4, the ratio of the longitudinal displacement at the surface of the plate u(h//2) to the displacement at the middle surface u(o) is plotted as a function of the ratio $\frac{h}{L}$. In correspondence to the value $\frac{h}{L} = 0.47$ nodal surfaces appear on the two surfaces of the plate.

In Fig. 5, the nondimensional ratios:

$$+\frac{u}{u(o)}, \frac{iv}{u(o)}, \pm\frac{\sigma_x}{\sigma_x(o)} \text{ and } \pm\frac{\sigma_y}{\sigma_x(o)}$$

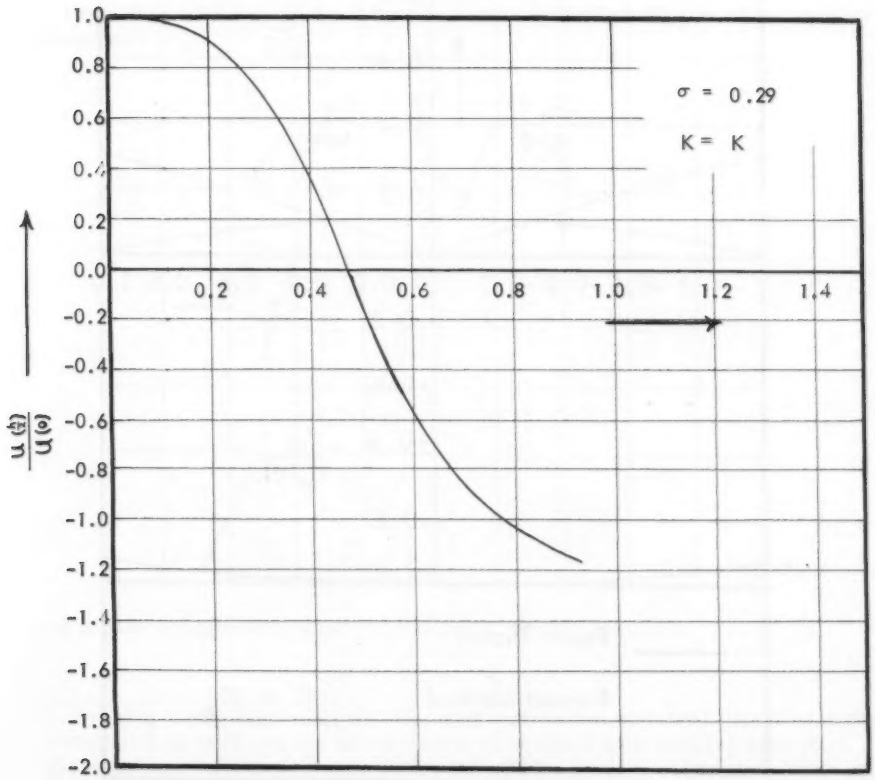

FIGURE 4

Ratio of displacement at the surface of the plate to the displacement at the middle surface expressed as a function of $(\frac{h}{L})$.

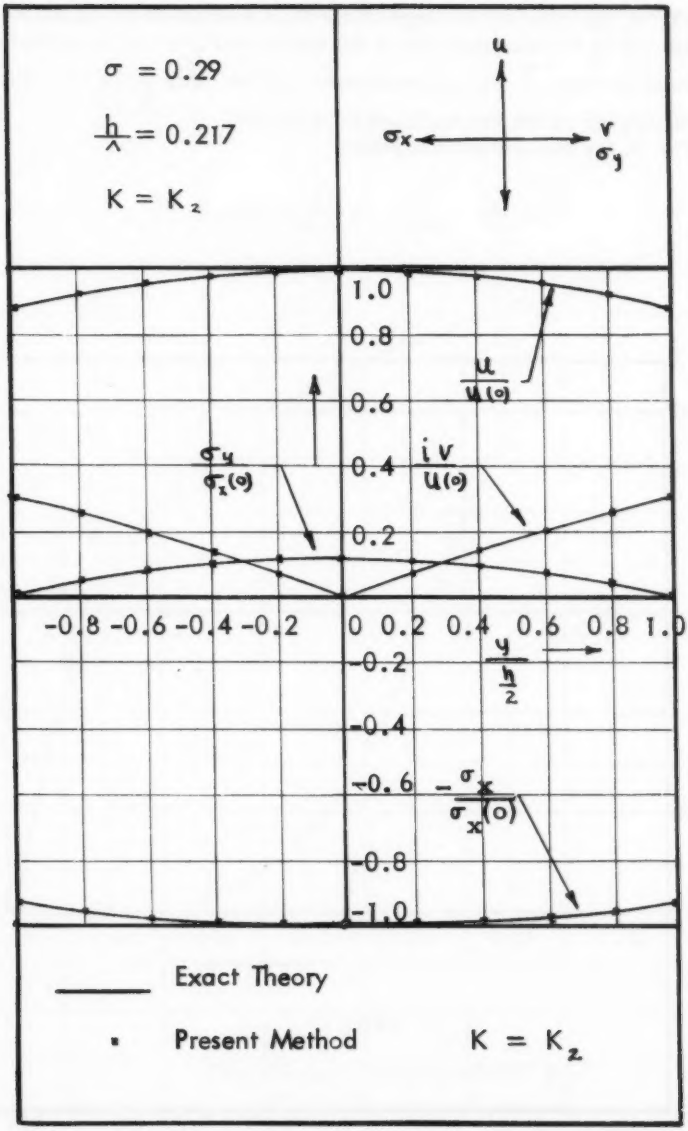

FIGURE 5

Variation of displacements and stresses over the cross-section of a plate of thickness h.

computed by the method presented in this paper for a value $\frac{h}{L} = 0.217$ using $K = K_2$ are compared with the numerical results computed by J. P. Marsden[3] from the exact theory given by Lamb.[2]*

In Figs. 6, 7, 8, 9, the above ratios are plotted as functions of the ratio $(\frac{y}{\frac{h}{2}})$ for different values of the ratio $\frac{h}{L}$.

Appendix

The Equations of Motion for Longitudinal Waves Derived by the Method of Internal Constraints

From Eqs. (1'), one derives for the components of strain the following expressions:

$$\varepsilon_x = \frac{\partial u}{\partial x} = \frac{\partial v_x}{\partial x} + \left(\frac{y}{\frac{h}{2}}\right)^2 \frac{\partial f_x}{\partial x}$$

$$\varepsilon_y = \frac{\partial v}{\partial y} = \lambda_y - \left(\frac{y}{\frac{h}{2}}\right)^2 \left[\lambda_y + \alpha\left(\frac{\partial v_x}{\partial x} + \frac{\partial f_x}{\partial x}\right)\right]$$

$$\varepsilon_z = \frac{\partial w}{\partial z} = 0$$

$$\gamma_{xy} = \frac{\partial u}{\partial y} + \frac{\partial v}{\partial x} = \frac{2y}{\left(\frac{h}{2}\right)^2} f_x + y \frac{\partial \lambda_y}{\partial x} - \frac{1}{3} \frac{y^3}{\left(\frac{h}{2}\right)^2} \frac{\partial}{\partial x} \left[\lambda_y + \alpha\left(\frac{\partial v_x}{\partial x} + \frac{\partial f_x}{\partial x}\right)\right]$$

$$\gamma_{xz} = \frac{\partial u}{\partial z} + \frac{\partial w}{\partial x} = 0$$

$$\gamma_{yz} = \frac{\partial v}{\partial z} + \frac{\partial w}{\partial y} = 0$$

and for the components of particle velocity, the expressions

---

*In drawing these diagrams, the following convection was used. Assuming the constant A is positive, the above ratios were taken with the plus sign when the displacements and stresses near the middle surface of the plate were of the form $+A(Re)e^{i\gamma(x-ct)}$ or $iA(Re)e^{i\gamma(x-ct)}$ where (Re) denotes a positive real number. If instead, the displacements and stresses were of the form $-A(Re)\, e^{i\gamma(x-ct)}$ and $-iA(Re)\, e^{i\gamma(x-ct)}$, the above ratios were taken with the minus sign.

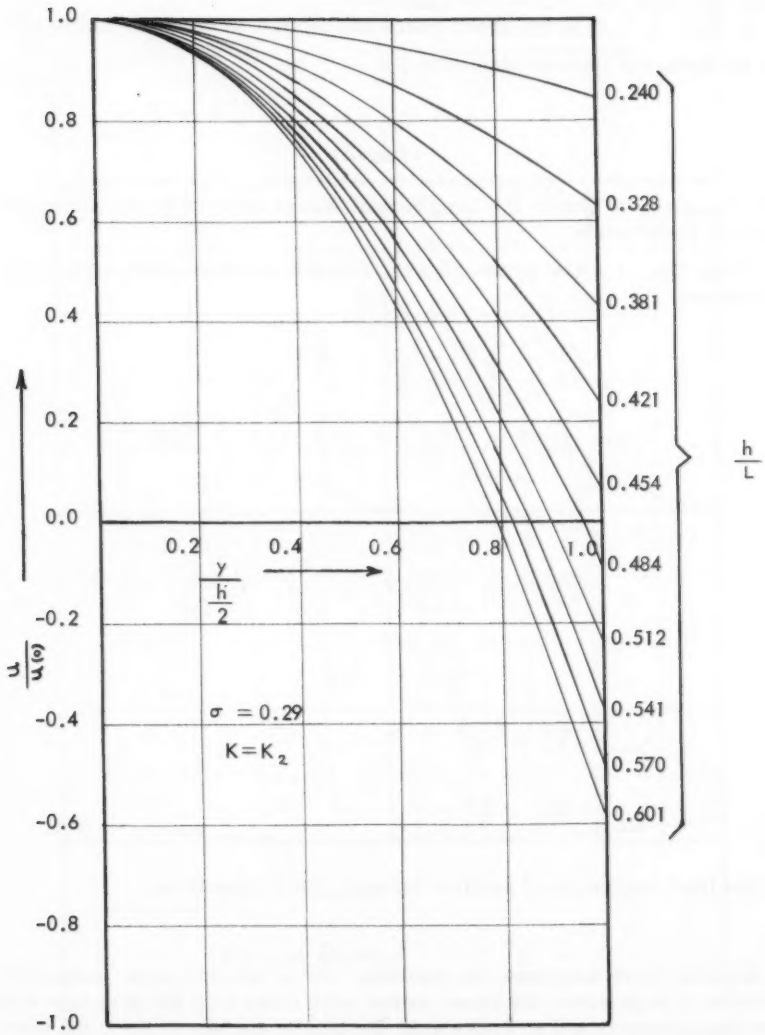

FIGURE 6

Variation of the longitudinal displacement over the cross-section of a plate of thickness h.

$$\frac{\partial u}{\partial t} = \frac{\partial v_x}{\partial t} + \left(\frac{y}{\frac{h}{2}}\right)^2 \frac{\partial f_x}{\partial t}$$

$$\frac{\partial v}{\partial t} = y \frac{\partial \lambda_y}{\partial t} - \frac{1}{3} \frac{y^3}{\left(\frac{h}{2}\right)^2} \frac{\partial}{\partial t} \left[\lambda_y + \left(\frac{\partial v_x}{\partial x} - \frac{\partial f_x}{\partial x}\right)\right] \qquad (17)$$

$$\frac{\partial w}{\partial t} = 0$$

In deriving the equations of motion, the factor K will be considered constant* so that γ_{xy} and $\frac{\partial v}{\partial t}$ can be written under the form

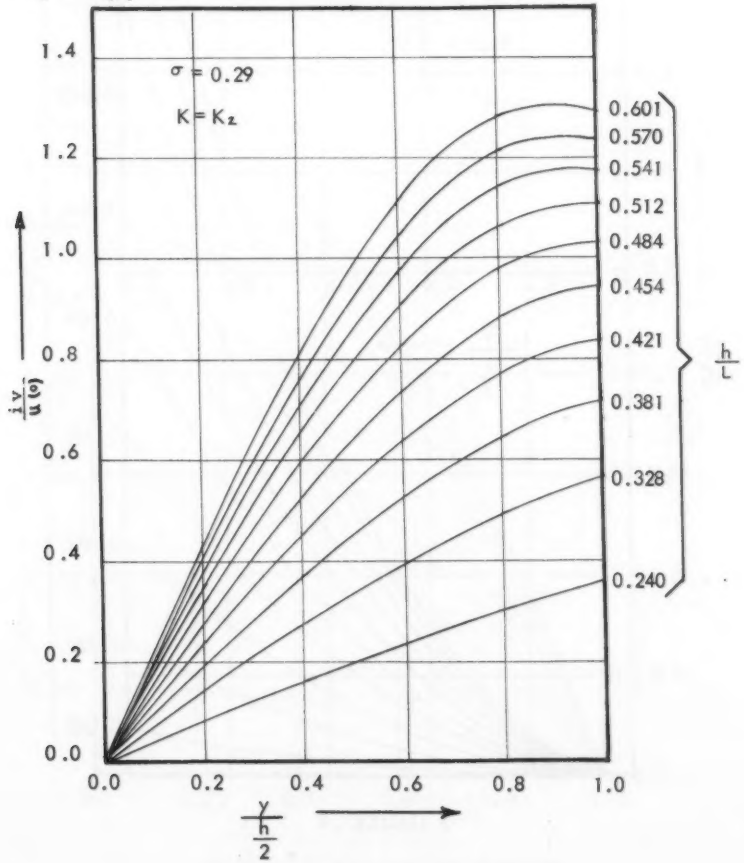

FIGURE 7

Variation of transverse displacement over the cross section of a plate of thickness h.

*The effect of the introduction of the factor K has been discussed in detail in the paper.

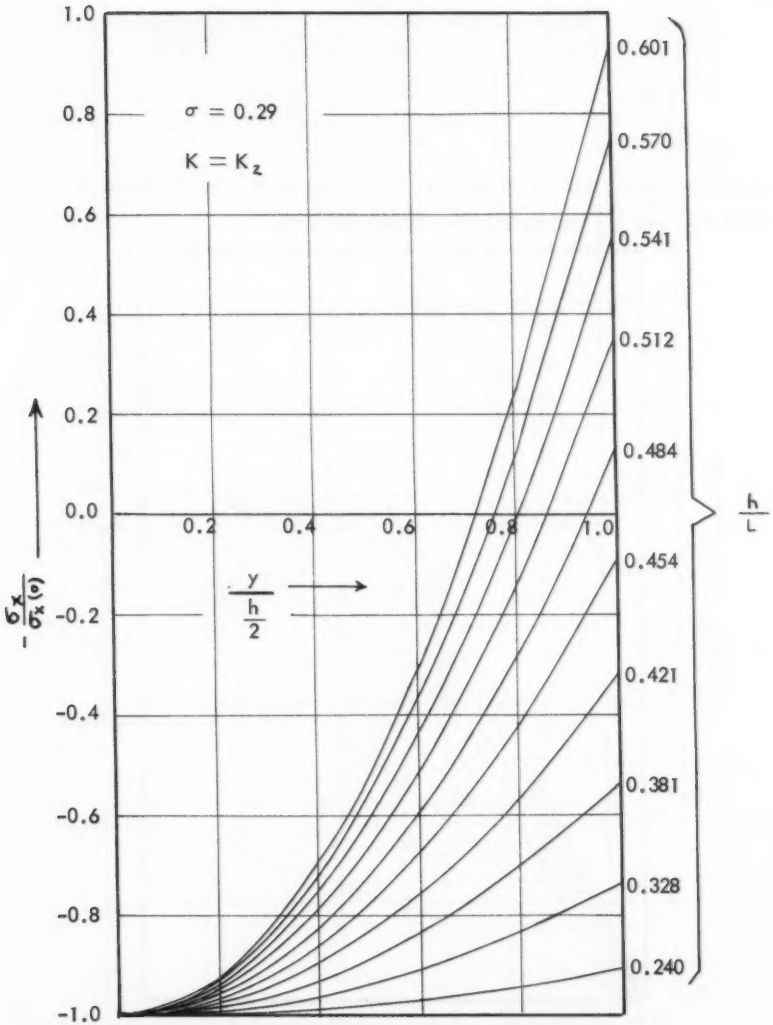

FIGURE 8

Variation of longitudinal stress over the cross-section of a plate of thickness h.

$$\gamma_{xy} = \frac{2y}{(\frac{h}{2})^2} f_x + y \frac{\partial \lambda_y}{\partial x} - \frac{1}{3} \frac{y^3}{(\frac{h}{2})^2} K \frac{\partial \lambda_y}{\partial x} \quad (18)$$

$$\frac{\partial v}{\partial t} = y \frac{\partial \lambda_y}{\partial t} - \frac{1}{3} \frac{y^3}{(\frac{h}{2})^2} K \frac{\partial \lambda_y}{\partial t} \quad (19)$$

The potential energy of the plate will be expressed by:

$$U = - \int_v \left\{ (\frac{\lambda}{2} + G) \left[\varepsilon_x^2 + \varepsilon_y^2 + 2\alpha \varepsilon_x \varepsilon_y \right] + \frac{G}{2} \gamma_{xy}^2 \right\} dV \quad (20)$$

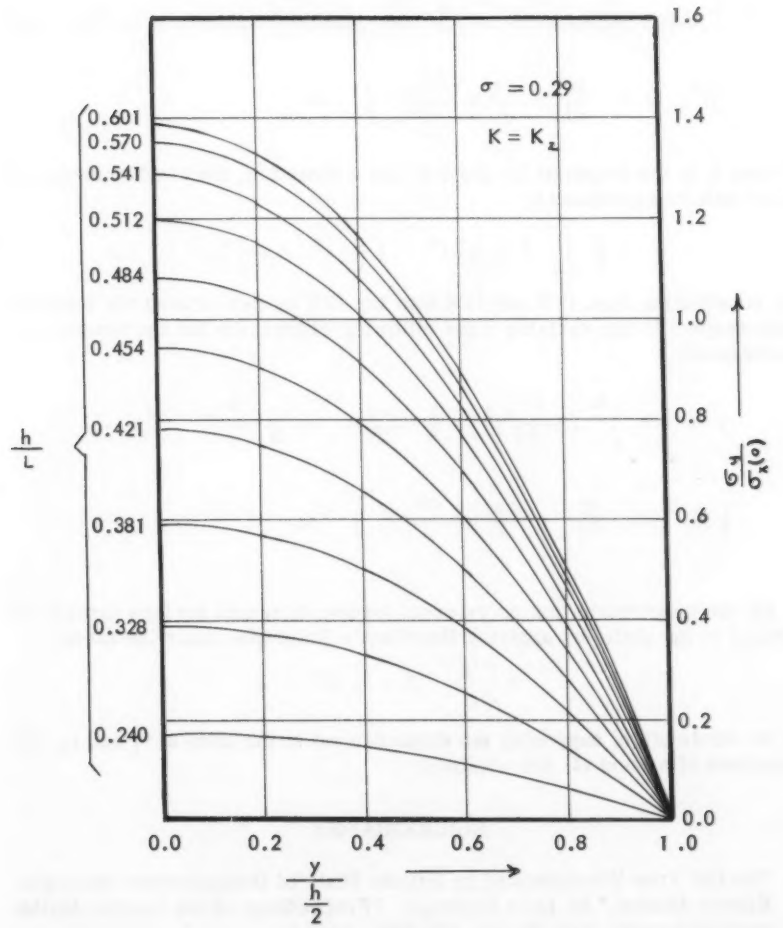

FIGURE 9

Variation of the transverse stress over the cross-section of a plate of thickness h.

where V is the volume of the plate. By substituting Eqs. (16) and (18) into Eq. (20) by performing the integration with respect to the variable y the following expression for the potential energy is obtained.

$$U = -h \int_0^L \left\{ \left(\frac{\lambda}{2} + G\right) \left[\left(1 - \frac{7}{15}\alpha^2\right)\left(\frac{\partial v_x}{\partial x}\right)^2 + \frac{1}{5}(1-\alpha^2)\left(\frac{\partial f_x}{\partial x}\right)^2 + \right.\right.$$

$$+ \frac{8}{15}\lambda_y^2 + \frac{2}{3}(1-\alpha^2)\frac{\partial v_x}{\partial x}\frac{\partial f_x}{\partial x} + \frac{8}{15}2\alpha\lambda_y \frac{\partial v_x}{\partial x}\Big] + \qquad (21)$$

$$+ \frac{G}{2}\left[\frac{4}{3} \frac{1}{\left(\frac{h}{2}\right)^2} f_x^2 + \frac{4}{3}\left(1 - \frac{K}{5}\right) f_x \frac{\partial \lambda_y}{\partial x} + \right.$$

$$\left.\left. + \left(\frac{h}{2}\right)^2 \frac{1}{3}\left(1 - \frac{K^2}{21} - \frac{2K}{5}\right)\left(\frac{\partial \lambda_y}{\partial x}\right)^2 \right]\right\} dx$$

Where L is the length of the plate in the x direction, the kinetic energy of the plate will be expressed by

$$T = \frac{\rho}{2} \int_V \left\{ \left(\frac{\partial u}{\partial t}\right)^2 + \left(\frac{\partial v}{\partial t}\right)^2 + \left(\frac{\partial w}{\partial t}\right)^2 \right\} dV \qquad (22)$$

By substituting Eqs. (17) and (19) into Eq. (22) by performing the integration with respect to the variable y the following expression for the kinetic energy is obtained:

$$T = \frac{\rho}{2} h \int_0^L \left\{ \left(\frac{\partial v_x}{\partial t}\right)^2 + \frac{1}{5}\left(\frac{\partial f_x}{\partial t}\right)^2 + \frac{2}{3}\frac{\partial v_x}{\partial t}\frac{\partial f_x}{\partial t} + \right.$$

$$\left. \frac{1}{3}\left(\frac{h}{2}\right)^2 \left(1 + \frac{K}{21} - \frac{2K}{5}\right)\left(\frac{\partial \lambda_y}{\partial t}\right)^2 \right\} dx \qquad (23)$$

On the assumption that no external forces (body and surface forces) are applied to the plate, by applying Hamilton's Principle under the form:

$$\delta \int_{t_1}^{t_2} (U + T)\, dT = 0$$

to the whole plate, supposing the displacement to the zero at t_1 and t_2, the equations of motion (4) are obtained.

BIBLIOGRAPHY

1. "On the Free Vibrations of an Infinite Plate of Homogeneous Isotropic Elastic Matter," by Lord Rayleigh. (Proceedings of the London Mathematical Society, Vol. 20, pp. 225-239. 1888.)

2. "On Waves in an Elastic Plate," by H. Lamb, (Proceedings of the Royal Society of London. Series A, Vol. 93, 1917, pp. 119-128.)

3. "Experiments on the Dispersion of Stress Waves," by J. P. Marsden (Thesis submitted to the University of Wales in candidature for the degree of Philosophical Doctor. April 1949 (not yet published.)

4. "Dispersion of Longitudinal Waves," by E. Volterra (Proc. Paper 1322, Journal of the Engineering Mechanics Division of the American Society of Civil Engineers, Vol. 83, No. E. M. 3, July 1957.)

5. "An Engineering Theory of Longitudinal Wave Propagation in Cylindrical Elastic Rods," by E. C. Zachmanoglou and E. Volterra (Presented at the Third U. S. National Congress of Applied Mechanics at Brown University in June 1958).

6. See: Applied Mechanics Reviews, Vol. 11, No. 74 (January 1958).

Journal of the
ENGINEERING MECHANICS DIVISION
Proceedings of the American Society of Civil Engineers

THE ELASTIC STABILITY OF THIN SPHERICAL SHELLS

Gideon P. R. von Willich,[1] A.M. ASCE

SUMMARY

Previous theoretical work relating to elastic buckling of thin spherical shells is reviewed. A theory, based on strain-energy considerations, is presented for determining buckling pressures of shallow thin spherical shells under external pressure, and it is suggested that the results may be extended to deeper shells.

INTRODUCTION

During recent years, shell-type structures have increased in popularity. Where light weight has been sought, the buckling characteristics of these types of construction have often been an important consideration. It is therefore not surprising that the question of elastic stability of shells has been of great interest to aircraft and missile designers. However, with the tendency in building construction towards the use of shallower and lighter shells, this problem is also becoming important to structural engineers.

Unfortunately, even simple physical phenomena relating to shells tend to lead to intricate and tedious mathematical analysis. This is especially the case in the investigation of buckling problems. This paper is therefore restricted to consideration of a single aspect, namely the elastic stability of thin spherical shells under external pressure.

Review of Previous Work

On page 491 of reference 6, Timoshenko describes the "classical" or linear buckling theory, together with a short history of the problem. In this approach

Note: Discussion open until June 1, 1959. To extend the closing date one month, a written request must be filed with the Executive Secretary, ASCE. Paper 1897 is part of the copyrighted Journal of the Engineering Mechanics Division, Proceedings of the American Society of Civil Engineers, Vol. 85, No. EM 1, January, 1959.

1. Princ. Research Officer, Mechanics Sub-div., National Mech. Eng. Research Inst., South African Council for Scientific and Industrial Research, Pretoria, Africa.

it is assumed that buckling will occur at a pressure which permits an equilibrium deflected shape that is infinitessimally removed from the trivial spherical shape. The method is thus analogous to the determination of the Euler buckling load of an initially straight strut under axial compression. This method of attack adopts the "eigenvalue" view of buckling, in which it is supposed that the structure retains its shape, undergoing only uniform contraction, until the critical load is reached. At this point, a deflected shape differing from the trivial one becomes possible. The linear theory does not allow the determination of the magnitude of the deflection at any point; with a constant buckling load, arbitrary amplitudes are permissible. In the case of a uniform strut, it is possible to obtain a solution of the governing differential equation using a more accurate expression for the curvature of the strut, and it is then found that the load does increase slowly with increasing lateral displacement, although at the start of buckling the rate of increase is zero. The analogous problem for the shell, with the use of more accurate expressions for curvature, is not readily solved, but it can be accepted that the equilibrium pressure decreases with increasing deflection, so that equilibrium configurations exist at pressures appreciably below the predicted buckling pressure. In this way, the behaviour of the shell differs essentially from that of the strut. Experimental evidence also shows that actual buckling pressures correspond closely with theoretical values in the case of struts, but in the case of spherical shells, the predicted buckling pressures are roughly between two and four times too high. The discrepancy in the latter case also extends to the buckled shape: the theory predicts that this will be in the form of a number of small waves covering the surface of the shell (all of which will be in unstable equilibrium under constant pressure), while in practice buckling is localized to a single "dimple" which grows progressively larger.

Several papers have been published in attempts to explain the discrepancies between theory and experiments.

Von Kármán and Tsien,[8] proposed the hypothesis that the practical buckling pressure of a spherical shell will correspond to the minimum pressure necessary to keep the shell in equilibrium in a buckled shape with finite deflection. However, Friedrichs[2] showed that certain assumptions made by these authors were unjustifiable as they seriously affected the results obtained, and that the hypothesis was not tenable. A subsequent paper by Tsien,[7] proposed new buckling criteria, namely:

1. The energy level (i.e. strain-energy in the shell plus potential energy of the applied pressure) must be the same before and after buckling, and

2. The geometric restraints of the loading procedure must be satisfied.

The theoretical predictions obtained by Tsien agreed well with experimental evidence. However, the criteria stated are open to question. The energy level of the shell obviously cannot be higher after buckling than before buckling, but there is no reason why it should not be lower. In fact, experimental observations show that the snap-through type of buckling in shells is generally accompanied by noticeable noise and vibration, indicating a definite energy loss. It is of course necessary that the loading conditions must be satisfied, but it is difficult to understand why they should affect the magnitude of the buckling load: they merely influence the behaviour of the shell after the maximum load has been reached. Tsien's theory distinguishes between shells

loaded by constant pressure (for instance in structures immersed at a great depth in a fluid) and those in which the pressure is reduced during testing (as is the case when a specimen is tested in a tank with liquid under pressure). Tests do not show a difference in the buckling pressures obtained by the two methods, and one cannot assume that the shell "knows" before it commences to buckle, what will happen to the load during the buckling process.

The "eigenvalue" approach was adopted in all these publications. This approach, with its supposition of discontinuous behaviour at the buckling load, applies to perfect structures, which are not attainable in practice. It is more logical to regard the buckling phenomenon as a loading process in which the relation between load and deflection is non-linear. In the case of the strut it is readily shown that the behaviour predicted by the "eigenvalue" procedure is the limiting case as imperfections tend to zero. However, it is doubtful whether this is true for a spherical shell, and the mathematical complexities of non-linear deformations of spherical shells make this question difficult if not impossible to settle.

The differential equations governing axi-symmetrical deflections of thin shells of revolution were given by E. Reissner,(5) the equilibrium equations and the stress-displacement equations being reduced to two simultaneous non-linear differential equations in two variables. The solution of the equations presents enormous mathematical difficulties, however. For the case of a shallow spherical shell of uniform thickness the form of the equations becomes much simpler, as some of the terms become negligible. The simplified equations are still difficult to solve, but significant progress has been made in obtaining series solutions, for instance by Kaplan and Fung,(3) Reiss, Greenberg and Keller,(4) and Archer.(1) However, a large number of terms in the series solutions are required to obtain convergence.

Several authors have reported experimental results, which are illustrated graphically in Figure 2. Tests were also carried out by W. Delano in the Civil Engineering Department of the Massachusetts Institute of Technology in 1953-54, under the supervision of Prof. C. H. Norris.

For shallow spherical shells clamped around the circumference, with given thickness and radius of curvature, the buckling pressure varies with the distance of the circumference from the axis. For a certain value of this distance, the buckling pressure will be a minimum, and it is felt that this minimum is of some significance in predicting the buckling pressure of the complete spherical shell.

Scope: The following analysis refers to shallow thin spherical shells; however, up to a certain stage, the equations are equally valid for other shallow thin shells of revolution, as this extra degree of generality can be conveniently introduced. By "shallow" and "thin" are meant that, respectively, the central rise and the shell thickness are small in comparison with the base diameter. The shell is assumed to be rigidly fixed around the boundary and to be subjected to uniform normal external pressure.

The thickness is assumed to be constant, and the material to be homogeneous and isotropic, and linearly elastic with the same modulus of elasticity in tension and compression. It is assumed that the elastic limit of the material is not exceeded. Deflections of the shell are assumed to be symmetrical about the axis.

The so-called Euler-Bernoulli hypothesis is adopted, i.e. it is assumed that normals to the middle surface of the shell before deformation remain

normal to the middle surface after deformation without extension.

Notation: Some of the symbols used are illustrated in the accompanying Figure 1. Others are defined where they first occur in the text. Cylindrical polar co-ordinates are used. For brevity, differentiation (partial or total) is denoted by a comma and a subscript, e.g.

$$w_{,r} = \frac{\partial w}{\partial r} \qquad w_{,rr} = \frac{\partial^2 w}{\partial r^2}$$

Strain Expressions

The following expressions for strains in terms of displacements can be derived on the assumptions that

$$z_{,r} \ll 1 \quad \text{and} \quad \frac{h}{r_o} \ll 1$$

and $$w = O(z_o)$$

Radial strain at middle surface

$$\epsilon_r = u_{,r} + z_{,r} w_{,r} + \frac{1}{2} w_{,r}^2 \tag{1}$$

Radial change in curvature

$$\kappa_r = - w_{,rr} \tag{2}$$

Circumferential strain at middle surface

$$\epsilon_\theta = \frac{u}{r} \tag{3}$$

Circumferential change in curvature

$$\kappa_\theta = - \frac{w_{,r}}{r} \tag{4}$$

Energy Expressions

The following relations for the three energy components are easily derived:

Strain-energy due to extension of the middle surface

$$U_e = 2\pi \frac{Eh}{2(1-\nu^2)} \int_0^{r_o} \left(\epsilon_r^2 + \epsilon_\theta^2 + 2\nu \epsilon_r \epsilon_\theta\right) r\, dr \tag{5}$$

Strain-energy due to bending

$$U_b = 2\pi \frac{Eh^3}{24(1-\nu^2)} \int_0^{r_o} \left(\kappa_r^2 + \kappa_\theta^2 + 2\nu \kappa_r \kappa_\theta\right) r\, dr$$

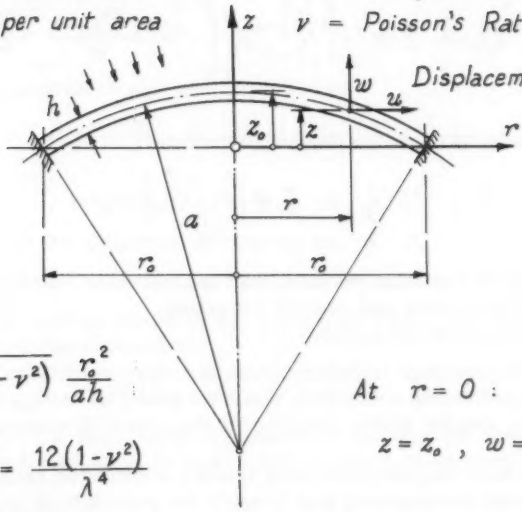

$$\lambda^2 = \sqrt{12(1-\nu^2)}\ \frac{r_o^2}{ah}$$

$$\eta = \frac{a^2h^2}{r_o^4} = \frac{12(1-\nu^2)}{\lambda^4}$$

At $r = 0$: $z = z_o$, $w = w_o$

$$P = \frac{1-\nu^2}{E}\left(\frac{r_o}{h}\right)^4 q \qquad W = \frac{w_o a}{r_o^2}$$

$$p = \frac{1}{2E}\ \frac{a^2}{h^2}\sqrt{3(1-\nu^2)}\ q = \frac{6\sqrt{3(1-\nu^2)}}{\lambda^4}\ P$$

q_{cr}, P_{cr}, p_{cr} are critical buckling values of q, P, p respectively.

ϵ_r = radial strain at middle surface

κ_r = radial change of curvature

ϵ_θ = circumferential strain at middle surface

κ_θ = circumferential change of curvature

Figure 1 : Notation

Provided that $w_{,r} = 0$ at $r = 0$ and $r = r_o$, the expression for U_b can be written

$$U_b = 2\pi \frac{Eh^3}{24(1-\nu^2)} \int_0^{r_o} r^3 \left(\frac{w_{,r}}{r}\right)_{,r}^2 dr \qquad (6)$$

The Potential Energy of the applied pressure is

$$U_p = 2\pi q \int_0^{r_o} w r\, dr \qquad (7)$$

The principle of minimum potential can be applied to find the relation between applied pressure and central deflection.

This principle can be stated:

Of all displacements satisfying given boundary conditions, those which satisfy the equilibrium conditions make the potential energy assume a stationary value, and for stable equilibrium the potential energy must be a minimum.

The procedure adopted here is to assume a deflected shape, containing certain unknown parameters, and to apply the principle of minimum potential to find these parameters.

For axi-symmetrical deformations of a shell of revolution, each element of the shell has two degrees of freedom, corresponding to the two displacement components. However, in using the strain-energy procedure in connection with an assumed deflected shape, it is sufficient to assume a suitable shape for the component w parallel to the shell axis. The optimum shape for the other component u can then be determined by means of a simple application of the calculus of variations.

The total potential

$$\Omega = U_e + U_b + U_p$$

Only U_e contains u, hence for a given w the condition for minimising Ω becomes $\delta U_e = 0$, which leads to the equilibrium equation.

$$\left[r\left(\epsilon_r + \nu\epsilon_\theta\right)\right]_{,r} - \left(\epsilon_\theta + \nu\epsilon_r\right) = 0$$

If the strain expressions are expressed in terms of displacements, as given by equations (1) and (3), the following differential equation is obtained:

$$r^2 u_{,rr} + r\, u_{,r} - u = -r^2\left(z_{,r} w_{,r} + \tfrac{1}{2} w_{,r}^2\right)_{,r} - r(1-\nu)\left(z_{,r} w_{,r} + \tfrac{1}{2} w_{,r}^2\right) \qquad (8)$$

For a given shell, z is a known function of r, and w is assumed in terms of r. The terms of the right hand side can therefore be expressed as a

function of r, and the differential equation can then be solved without difficulty.

If the right hand side of equation (8) can be written as a polynomial in r, of the form

$$B_0 + B_1 r + B_2 r^2 + \ldots + B_n r^n$$

then the general solution of equation (8) becomes

$$u = Ar - B_0 + \tfrac{1}{2} B_1 r \log_e r + \tfrac{1}{3} B_2 r^2 + \tfrac{1}{8} B_3 r^3 + \ldots + \frac{1}{n^2-1} B_n r^n$$

From the nature of the deflection component and of z, it is found that $B_0 = B_1 = 0$, and in fact that u contains only odd powers of r. The constants B will be known in any particular case, and A must be found from the boundary condition

$$u = 0 \quad \text{at} \quad r = r_0 .$$

Up to this point the analysis is applicable to thin shallow shells of revolution; the subsequent analysis is restricted to spherical segments only.

Assumed Deflected Shape:

The shell is assumed to deflect in the form

$$w = w_0 \left[1 + C_2 \left(\frac{r}{r_0}\right)^2 + C_4 \left(\frac{r}{r_0}\right)^4 + C_6 \left(\frac{r}{r_0}\right)^6 \right]$$

To satisfy the boundary conditions at $r = r_0$, namely $w = 0$ and $w_{,r} = 0$, this becomes

$$w = w_0 \left[1 + (C-2)\left(\frac{r}{r_0}\right)^2 - (2C-1)\left(\frac{r}{r_0}\right)^4 + C\left(\frac{r}{r_0}\right)^6 \right] .$$

For the shallow spherical shell,

$$z = \frac{1}{2a}(r_0^2 - r^2)$$

and hence,

For $\nu = 0.3$

$$\Omega = 2\pi \left\{ \frac{Eh}{2(1-\nu^2)} \frac{w_0^2 r_0^2}{a^2} \left[\frac{13}{144000}(113C^2 + 856C + 2048) + \frac{w_0 a}{r_0^2} \frac{13}{12000}(7C^3 + 50C^2 + 118C + 360) \right] \right.$$

$$+\frac{w_o^2 a^2}{r_o^4}\frac{13}{1980000}(271C^4+748C^3+7392C^2+6820C+31900)$$
$$+\frac{a^2h^2}{r_o^4}\frac{4}{45}(4C^2+5C+10)\Big]+q\frac{w_o r_o^2}{24}(C+4)\Big\} \qquad (9)$$

For $\nu = 0$

$$\Omega = 2\pi\left\{\frac{Eh}{2(1-\nu^2)}\frac{w_o^2 r_o^2}{a^2}\left[\frac{1}{10080}(83C^2+616C+1568)\right.\right.$$
$$+\frac{w_o a}{r_o^2}\frac{1}{840}(5C^3+38C^2+82C+280)$$
$$+\frac{w_o^2 a^2}{r_o^4}\frac{1}{138600}(205C^4+484C^3+5808C^2+4180C+25300)$$
$$\left.+\frac{a^2h^2}{r_o^4}\frac{4}{45}(4C^2+5C+10)\right]+q\frac{w_o r_o^2}{24}(C+4)\Big\} \qquad (10)$$

Determination of Critical Pressure

Strict application of the principle of minimum potential implies that the correct approach is to minimise Ω with respect to the two variables C and w_o, i.e. to set $\Omega_{,C} = 0$ and $\Omega_{,w_o} = 0$. However, this gives rise to great arithmetical complications, and a simpler approach is adopted. The parameter C is assumed to be a constant for a given shell, and its value is found from the condition that the buckling pressure is a minimum, i.e. $\Omega_{,w_o} = 0$ and $P_{cr,C} = 0$.

For $\nu = 0.3$: The equation resulting from putting $\Omega_{,w_o} = 0$ in equation (9) may be written more compactly by setting:

$$P = \frac{1-\nu^2}{E}\left(\frac{r_o}{h}\right)^4 q \qquad F_1 = 113C^2+856C+2048$$

$$F_2 = 7C^3+50C^2+118C+360$$

$$W = \frac{w_o a}{r_o^2} \qquad F_3 = 271C^4+748C^3+7392C^2+6820C+31900$$

$$\eta = \frac{a^2h^2}{r_o^4} \qquad F_4 = 4C^2+5C+10$$

Then:

$$P(C+4) = -\frac{39}{250}\left(\frac{1}{\eta}\right)^{\frac{3}{2}} W\left(\frac{1}{72}F_1 + \frac{1}{4}F_2 W + \frac{1}{495}F_3 W^2 + \frac{1600}{117}F_4\eta\right) \tag{11}$$

The condition for buckling is $P_{,W} = 0$, which gives

$$\frac{1}{72}F_1 + \frac{1}{2}F_2 W + \frac{1}{165}F_3 W^2 + \frac{1600}{117}F_4\eta = 0$$

the appropriate value of W being given by the smaller of the two roots.

Then

$$W = -\frac{165}{4}\frac{1}{F_3}\left(F_2 - \sqrt{F_2^2 - \frac{2}{1485}F_1F_3 - \frac{5120}{3861}\eta F_3F_4}\right) \tag{12}$$

and the value of P_{cr} can be found by substituting this into equation (11).

For a given value of λ and hence of η, the optimum value of C can be found, in theory, by setting $P_{cr,C} = 0$. However, because of the complexity of the resulting equation, it was found more convenient to determine the minimum value of P_{cr} with the corresponding value of C by a trial and error process.

For $\nu = 0$, the corresponding equations are as follows:

With

$$P = \frac{1-\nu^2}{E}\left(\frac{r_o}{h}\right)^4 q$$

$$W = \frac{w_o a}{r_o^2}$$

$$\eta = \frac{a^2h^2}{r_o^4}$$

$$F_1 = 83C^2 + 616C + 1568$$

$$F_2 = 5C^3 + 38C^2 + 82C + 280$$

$$F_3 = 205C^4 + 484C^3 + 5808C^2 + 4180C + 25300$$

$$F_4 = 4C^2 + 5C + 10$$

Setting $\Omega_{,w_o} = 0$ in equation (10) yields

$$P(C+4) = -\frac{6}{35}\left(\frac{1}{\eta}\right)^{\frac{3}{2}} W\left(\frac{1}{72}F_1 + \frac{1}{4}F_2 W + \frac{1}{495}F_3 W^2 + \frac{112}{9}F_4\eta\right) \tag{13}$$

and setting $P_{,W} = 0$ in this gives

$$\frac{1}{72}F_1+\frac{1}{2}F_2W+\frac{1}{165}F_3W^2+\frac{112}{9}F_4\eta=0$$

and solving for W

$$W=-\frac{165}{4}\frac{1}{F_3}\left(F_2-\sqrt{F_2^2-\frac{2}{1485}F_1F_3-\frac{1792}{1485}F_3F_4\eta}\right) \quad (14)$$

The numerical procedure adopted for the determination of the critical pressures from the preceding equations, was to calculate for various values of C, the corresponding values of P_{cr} until a situation was reached in which for three successive values of C, differing by 0.1, the value of P_{cr} corresponding to the middle value was smaller than the other two. As an additional refinement, the P_{cr}: C relation was approximated by a second degree polynomial for these three points, and the final value of P_{cr} was found from the minimum of this polynomial. It appeared, however, that this additional procedure was of more value in determining the final value of C than of P_{cr}, as near the minimum P_{cr} does not vary appreciably.

Results

The results of the calculations are given in Table 1. Here P_{cr} and p_{cr} are dimensionless forms for expressing the critical buckling pressure. The form $P_{cr}=\frac{1-\nu^2}{E}\left(\frac{r_o}{h}\right)^4 q_{cr}$ was used by Kaplan and Fung,[2] while p_{cr} is simply the ratio of the buckling pressure to that given by the linear buckling theory for the complete sphere, i.e.

$$p_{cr}=\frac{1}{2E}\frac{a^2}{h^2}\sqrt{3(1-\nu^2)}\;q_{cr}$$

$$=\frac{6\sqrt{3(1-\nu^2)}}{\lambda^4}\;P_{cr}$$

Comparison with Available Experimental Data

Figures 2 and 3 show the comparison of the experimental results with the calculated values given in Table 1 and with other published theoretical treatments.

It can be seen that the method used here gives a fairly good approximation to the experimental buckling loads for the range $\lambda = 3.5$ to $\lambda = 7.0$. For

λ	η	C	P_{cr}	p_{cr}
	$\nu = 0.3$			
3.5	0.072 77	- 0.72	9.00	0.595
4.0	0.042 66	- 1.09	14.02	0.543
4.5	0.026 63	- 1.43	22.19	0.537
5.0	0.017 47	- 1.74	33.86	0.537
6.0	0.008 426	- 2.06	73.37	0.561
7.0	0.006 031	- 2.40	149.38	0.617
8.0	0.002 666	- 2.53	292.59	0.708

Minimum $p_{cr} = 0.536$, with $\lambda = 4.75$

	$\nu = 0$			
3.5	0.079 97	- 0.28	8.33	0.577
4.0	0.046 88	- 0.89	12.05	0.489
4.5	0.029 26	- 1.21	18.74	0.475
5.0	0.019 20	- 1.53	28.74	0.478
6.0	0.009 259	- 1.96	63.40	0.508
7.0	0.004 998	- 2.23	131.05	0.567
8.0	0.002 930	- 2.38	257.63	0.654

Minimum $p_{cr} = 0.474$, with $\lambda = 4.66$

THEORETICAL RESULTS

Table 1

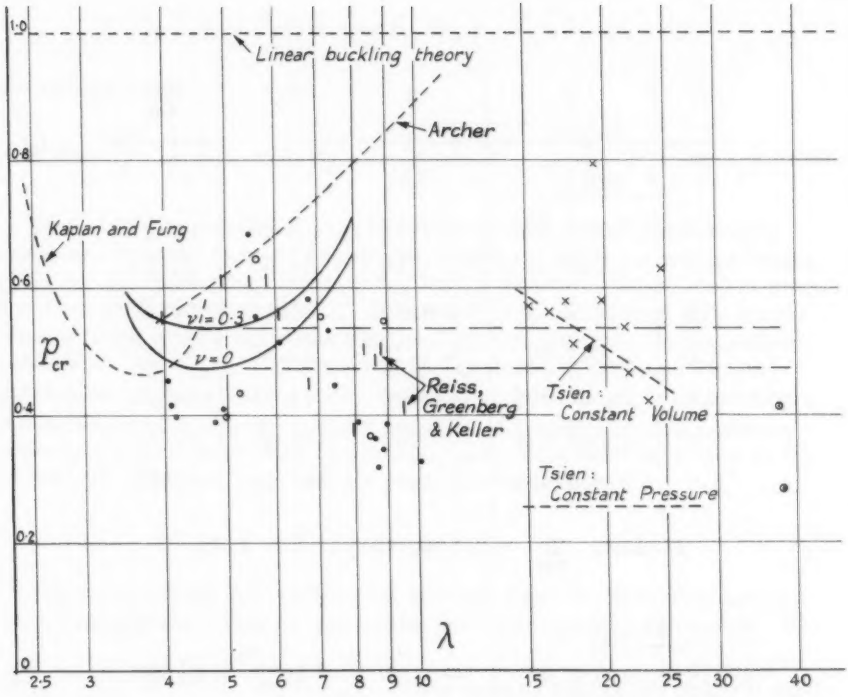

Previous theoretical results ----- and |

Present theoretical results ——

Test Results:

Tsien ×

Kaplan and Fung :

Hydraulic •

Air Pressure ○

Delano •

Comparison of Theoretical and Experimental Results

Figure 2

higher values of λ the theoretical predictions are too great. The experimental results show such a wide scatter that an accurate comparison is of course not possible. The prediction by this method in the range of λ mentioned can therefore be considered to be satisfactory.

The present method, as can be noted, compares well with previously published theoretical treatments.

Experimental evidence tends to show that buckling of deep spherical shell is characterised by the formation of a small indentation which grows progressively larger. The difference between this indentation and a shallow spherical

Comparison of Theoretical and Experimental Results
Figure 3

shell, clamped around the edge, lies in the different boundary conditions. It is illogical to suppose, as the theory predicts, that the buckling load of a shell will increase as the distance from the centre to the clamped boundary becomes larger. Hence, as an approximation, the hypothesis can be advanced that the buckling pressure for any depth of shell will be the same as that for the shallow shell, with the same thickness and curvature, whose boundary distance is such that the buckling pressure is a minimum.

It can be seen from Figure 2 that the minimum buckling pressure so defined gives a reasonable approximation for the buckling loads for all the experimental results.

This tentative theory may also be extended to shells which are not spherical, in which case the actual buckling pressure q_{cr} is reduced to the dimensionless form p_{cr} by using the maximum radius of curvature of the shell in the appropriate formula. The experimental results obtained by W. Delano at M.I.T. give the following comparison:

	p_{cr}	
	Experimental	Theoretical
Shallow ellipsoid	0.541, 0.498	0.536
Deep ellipsoid	0.218, 0.457	

It can be seen that the theoretical value, based on the assumption that $\nu = 0.3$, agrees reasonably well with three of the four experimental results. (The discrepancy in the remaining result was due to an imperfection in the manufacture of the specimen).

ACKNOWLEDGMENTS

This paper is based on material submitted in partial fulfillment of the requirements for the degree of Sc.D. at the Massachusetts Institute of Technology: the author is indebted to Professor Charles H. Norris, Professor of Structural Engineering, for his guidance, and to Professor John B. Wilbur, Head of the Department of Civil and Sanitary Engineering, for permission to publish this paper. The author also wishes to express his appreciation to the South African Council for Scientific and Industrial Research, whose award of a Senior Bursary helped to make this investigation possible, for their consent to the publication of the work.

BIBLIOGRAPHY

1. Archer, R. R. Stability limits for a clamped spherical shell segment under uniform pressure. Quarterly of Applied Mathematics, Vol. XV, No. 4 (1958).

2. Friedrichs, K. O. On the minimum buckling load for spherical shells. Theodor von Kármán Anniversary Volume, California Institute of Technology (1941).

3. Kaplan, A. and Fung, Y. C. A nonlinear theory of bending and buckling of thin elastic shallow spherical shells. National Advisory Committee for Aeronatics, Technical Note 3212 (1954).

4. Reiss, E. L., Greenberg, H. J., and Keller, H. B. Nonlinear deflections of shallow spherical shells. Journal of the Aeronautical Sciences, Vol. 24, No. 7 (1957).

5. Reissner, E. On axisymmetrical deformations of thin shells of revolution. Proceedings of Symposium on Applied Mathematics, American Mathematical Society, Vol. 3 (1950).

6. Timoshenko, S. Theory of Elastic Stability. McGraw-Hill Book Co., Inc. (1936).

7. Tsien, H.-S. A theory for the buckling of spherical shells by external pressure. Journal of the Aeronautical Sciences, Vol. 9, No. 10 (1942).

8. Von Kármán, Th. and Tsien, H.-S. The buckling of spherical shells by external pressure. Journal of the Aeronautical Sciences, Vol. 7, No. 2. (1939).

Journal of the
ENGINEERING MECHANICS DIVISION
Proceedings of the American Society of Civil Engineers

SIMPLIFICATION OF DIMENSIONAL ANALYSIS[a]

Charles C. Bowman[1] and Vaughn E. Hansen,[2] M. ASCE

Dimensional analysis is a powerful tool. Variables of a given problem are combined to form dimensionless parameters which can be grouped into meaningful functional equations. However, the standard method of deriving the dimensionless parameters using determinantes to form simultaneous equations is a rather tedious procedure. Considerable simplification results when the following steps are used singly or in combination: (1) Special arrangement of the variables in the determinant form, (2) Selection of repeating variables to represent the dynamic, kinematic and geometric variables.

Before using dimensional analysis the engineer must be familiar with the mechanics of the field in which he is working. He must realize dimensional analysis provides a partial solution without revealing the inner phenomena which may occur. It is a systematic treatment yielding an equation which is dimensionally correct. The dimensionless coefficients which are formed can be used to obtain similarity between model and prototype.

Conventional Determinant Method

The standard procedure of solution can be illustrated by analyzing the drag on a ship. The drag force F depends on the speed of the ship V, length of the ship L, the viscosity μ, the mass density ρ, and the acceleration of gravity, g. These variables can be related in functional form as $f(F, V, L, \mu, \rho, g) = 0$.[3]

Note: Discussion open until June 1, 1959. To extend the closing date one month, a written request must be filed with the Executive Secretary, ASCE. Paper 1898 is part of the copyrighted Journal of the Engineering Mechanics Division, Proceedings of the American Society of Civil Engineers, Vol. 85, No. EM 1, January, 1959.

a. Developed as a special problem in the Civil and Irrigation Engineering Dept., Spring Quarter, 1957, at Utah State University, Logan, Utah.

1. Asst. Prof., Agri. Eng. Dept., Montana State College, Bozeman, Mont.
2. Prof., Civ. and Irrig. Eng., Utah State Univ., Logan, Utah.

3. The purpose of this paper is to show the arrangement and handling of the variables rather than justifying the selection of variables. For a clear treatise of the selection of variables refer to Langhaar, Dimensional Analysis and Theory of Models, 1951, John Wiley and Son, pp. 21.

Seven steps are used to illustrate briefly how the determinant form is used to solve the simultaneous equations and to obtain the form of the dimensionless parameters. After they have been formed in the conventional manner, the utility of the simplifying steps will be shown.

Step 1: Forming the Matrix

To obtain the dimensionless parameters, first place the variables involved at the heads of the columns of the matrix. The dependent variable is placed at the head of the left hand column, followed on the right side by the variable which is easiest to regulate experimentally. This in turn is followed by the next easiest and so on. The dimensions of the variables are placed on the left side of the matrix forming the rows. The exponents of the dimensions for each of the variables are entered under the variables opposite the dimensions. Positive numbers are used for exponents appearing in the numerators and negative numbers for the exponents appearing in the denominators.

	F	V	L	μ	ρ	g
F	1	0	0	1	1	0
L	0	1	0-	2-	4	1
T	0-	1	0	1	2-	2

Step 2: Determining the Number of Dimensionless Parameters

Determine the number of dimensionless parameters which will appear by subtracting the number of dimensions from the number of variables. In the case being considered six variables appear along the top of the matrix and three dimensions along the side. Thus (n-r) = 6-3=3. Therefore, there will be three dimensionless parameters when the variables are properly combined.

Step 3: Obtaining Equations for the Dimensions

Assign K values to all variables, K_1 corresponds to F, K_2 corresponds to V, K_3 corresponds to L, K_4 corresponds to μ, K_5 corresponds to ρ, and K_6 corresponds to g.

	K_1	K_2	K_3	K_4	K_5	K_6
	F	V	L	μ	ρ	g
F	1	0	0	1	1	0
L	0	1	1	-2	-4	1
T	0	-1	0	1	2	-2

By solving for K_4, K_5 and K_6 in terms of K_1, K_2 and K_3, coefficients are established which force K_1, K_2 and K_3 to equal K_4, K_5 and K_6 respectively, thus causing the F, L and T rows to be dimensionless. Since in a dimensionally homogeneous equation the dimensions of force, length, and time are all equal to zero, the following equations can be obtained from the above matrix.

$$F: \quad K_1 + K_4 + K_5 = 0 \tag{2}$$

$$L: \quad K_2 + K_3 - 2K_4 - 4K_5 + K_6 = 0 \tag{3}$$

$$T: \quad -K_2 + K_4 + 2K_5 - 2K_6 = 0 \tag{4}$$

Solving eq. 2, 3, and 4 for K_4, K_5, and K_6 in terms of K_1, K_2, and K_3, the following equations are obtained:

$$K_4 = -2K_1 - 1/3K_2 - 2/3K_3 \tag{5}$$

$$K_5 = K_1 + 1/3K_2 + 2/3K_3 \tag{6}$$

$$K_6 = -1/3K_2 + 1/3K_3 \tag{7}$$

Step 4: Setting up a Matrix for Dimensionless Parameters

Set up a new matrix for the K values listing the K values at the head of the columns in their original order. The three dimensionless parameters are represented on the left side of the matrix by π_1, π_2 and π_3. Any values can be substituted for K_1, K_2 and K_3 where K_4, K_5 and K_6 are solved in terms of the first three K values and the parameters will be dimensionless. However, it is convenient to set $K_1 = 1$, $K_2 = 0$, and $K_3 = 0$ for π_1; $K_1 = 0$, $K_2 = 1$ and $K_3 = 0$ for π_2; and $K_1 = 0$, $K_2 = 0$, and $K_3 = 1$ for π_3. By substituting these values into equations 5, 6 and 7 the values of K_4, K_5 and K_6 for various π values can be entered in a matrix as shown below.

	K_1 F	K_2 V	K_3 L	K_4 μ	K_5 ρ	K_6 g
π_1	1	0	0	-2	1	0
π_2	0	1	0	-1/3	1/3	-1/3
π_3	0	0	1	-2/3	2/3	1/3

Step 5: Forming Dimensionless Parameters

The dimensionless parameters can now be read directly by reading from the π factors to the right along the rows. The exponential factors for each of the variables can be read off directly and placed in the numerator or denominator according to the sign. Thus obtaining the following parameters:

$$\pi_1 = \frac{F\,\rho}{\mu^2} \qquad \pi_2 = \frac{V\,\rho^{1/3}}{\mu^{1/3}\,g^{1/3}} \qquad \pi_3 = \frac{L\,\rho^{2/3}\,g^{1/3}}{\mu^{2/3}}$$

which combine into the following functional equation:

$$f_1(\pi_1, \pi_2, \pi_3) = 0 \tag{8}$$

Step 6: Securing Identifiable Parameters

The existing parameters are valid and equation 8 is correct, but the parameters are not readily identifiable in their present form. The parameters should be cleared of the fractional exponents and combined in the form of a product or a quotient to obtain identifiable numbers. The following

combinations form Reynolds number, Froude number and Euler number:

$$\frac{\pi_1}{\pi_2^2\,\pi_3^2} = \frac{F}{\rho V^2 L^2} = N_e \quad \pi_2 \times \pi_3 = \frac{VL\rho}{\mu} = N_r \quad \frac{\pi_2^2}{\pi_3} = \frac{V^2}{Lg} = N_f$$

which combined also form a valid functional equation

$$f_2 (N_e, N_r, N_f) = 0 \tag{9}$$

Step 7: Evaluating the Force on the Ship

To find the force on the ship, it is necessary to write eq. 9 so that the parameter containing force is explicit. This parameter is the Euler number.

$$N_e = f_3 (N_r, N_f) \tag{10}$$

but since $$N_e = \frac{F}{\rho V^2 L^2}$$

$$F = f_4 (N_r, N_f)\, \rho V^2 L^2 \tag{11}$$

This equation states that F is equal to a function of (N_r, N_f) times $\rho V^2 L^2$. The L^2 can be replaced by the cross sectional area A of the boat, which is determined by the design of the ship below the water line.[4] The $f_4(N_r, N_f)$ can be represented by a dimensionless coefficient called a drag coefficient designated by $C_d/2$. By substituting these values into equation 5 the following conventional drag equation results:

$$F = C_d A \frac{\rho V^2}{2} \tag{12}$$

Simplifying the Matrix Method of Solution

The conventional method used above is a long but useful method and can be used when many variables are involved and the identities of the parameters are unknown before hand. Due to the many steps the chance for error is great. This method can be simplified and shortened by the arrangement of the variables in step one. In this particular problem, it is realized the Reynolds number, Froude number and Euler number may be present in some form. Select variables which will appear only in one of the three dimensionless parameters, and place these variables at the head of the first three columns. The last 3 columns (this being a six-variable problem, are headed by) one dynamic, one geometric, and one kinematic repeating variable since all three types of variables are represented in the problem. The dynamic variable represents the force dimension, the geometric represents the length, and the kinematic the time.

It is convenient at this point to solve for the repeating variables (V, L, ρ) in terms of the non-repeating variables (μ, g, F) without resorting to the K terms which were used in the first solution. Thus using the original matrix form with the suggested changes in order of listing,

4. Vennard, Elementary Fluid Mechanics, Third Edition, John Wiley and Sons, 1956, pp. 341.

	μ	g	F	V	L	ρ
F	1	0	1	0	0	1
L	-2	1	0	1	1	-4
T	1	-2	0	-1	0	2

By solving for the repeating variables in terms of the non-repeating variables the following equations are obtained, remembering that the dimensions of the variables are represented in the equations and not the numerical values of the variables:

$$V = -\mu - 2g - 2F \tag{13}$$

$$L = -\mu + g - 2F \tag{14}$$

$$\rho = -\mu - F \tag{15}$$

Using these equations to form a second matrix and using N in place of the π for identifying the dimensionless parameters gives the following results:

	μ	g	F	V	L	ρ
N_1	1	0	0	-1	-1	-1
N_2	0	1	0	-2	1	0
N_3	0	0	1	-2	-2	-1

From this matrix the dimensionless parameters can be read directly.

$$N_1 = \frac{\mu}{V\,L\,\rho} \qquad N_2 = \frac{Lg}{V^2} \qquad N_3 = \frac{F}{V^2\,L^2\,\rho}$$

The readily recognized ratios of Reynold, Euler and Froude numbers are obtained merely by inverting N_1, N_2, and N_3. Hence,

$$N_r = \frac{VL\,\rho}{\mu} \qquad N_f = \frac{V^2}{Lg} \qquad N_e = \frac{V^2L^2\,\rho}{F}$$

Hence equation 10

$$N_e = f_3\,(N_r, N_f) \tag{10}$$

is obtained without having to find a combination of parameters which will form recognizable numbers.

This second solution proves two important points. (1) The arrangement of the variables can simplify the solution of dimensional analysis. (2) Repeating variables must be selected which have the dimensions necessary to cancel out the dimensions of the non-repeating variables. When F, L and T appear in the non-repeating variables it is necessary to have one dynamic, one kinematic, and one geometric variable in the repeating variables to form the dimensionless parameters.

When the number of parameters have been determined by (n-r) as previously discussed, it also indicates there will be (n-r) variables which will appear alone in each of the dimensionless parameters. The (n-r) variables which will appear alone may not be evident initially. The unknown variables will be forced to form a dimensionless parameter. Those variables which

are known to appear alone are placed first in the matrix followed by the variables which cannot be identified as part of a known number and these in turn are followed by one dynamic, one kinematic, and one geometric repeating variable which are known to appear in more than one of the dimensionless parameters.[5] The parameter probably, although not necessarily, will form identifiable numbers but they will be valid dimensionless parameters,which are characteristic of the problem being solved.

Simplified Dimensional Analysis

The above observation introduces a new simplification to the procedure of forming dimensionless parameters. By using the original problem of the drag on a ship which is a function of (F, V, L, μ, ρ, g) the simplification can be made quite evident. There are six variables present which are made up of three dimensions, F, L and T. Since (n-r) equals 3, there are three possible dimensionless parameters formed from the above variables. By examination and knowledge of the problem it is known that μ will appear in the Reynolds number and g will appear in the Froude number, thus leaving one parameter unknown. By selecting one dynamic, one kinematic and one geometric repeating variables which are known to appear in both of the known parameters, the third non-repeating variable can be determined. It is known that V, L appears in both the Reynold and Froude numbers. Therefore, it is safe to use them as two of the required three repeating variables.

The variable V represents the kinematic variables involving time and L is representative of the geometric variables involving length. A third dynamic variable is needed.

The Reynold number gives the third repeating variable because this number is characteristic of viscosity. Hence, the viscosity would not be repeating. Density ρ which appears in the number must be the other repeating variable. Thereby, the three repeating variables (V, L, ρ) have been selected leaving the variables (μ, g, F) as the non repeating variables.

To form the parameter, first select one of the non-repeating variables in quotient form such as μ, then combine this variable with any or all of the three repeating variables in such a way that the combination has zero dimensions. The following shows how this is done.

Since μ has a dimension of force, divide by the dynamic repeating variable to cancel the force dimension F.

$$\frac{\mu}{\rho} = \frac{FT}{L^2} \times \frac{L^4}{FT^2} = \frac{L^2}{T}$$

Dividing this ratio by the kinematic repeating variable V will remove the time dimension T.

$$\frac{\mu}{\rho V} = \frac{L^2}{T} \times \frac{T}{L} = L$$

Dividing by the geometric repeating variable L will remove the length dimension L.

---

5. If only dynamic and kinematic variables are involved, only one dynamic and one kinematic repeating variable would be used.

$$\frac{\mu}{\rho VL} = \frac{L}{L} = \text{zero dimensions} = N_r \text{ (Reynolds number)}$$

Repeating the above steps for the remaining non-repeating variables gives the following parameters:

$$g = \frac{L}{T^2}$$

Divide by V squared eliminates time

$$\frac{g}{V^2} = \frac{L}{T^2} \times \frac{T^2}{L^2} = \frac{1}{L}$$

Multiplying by L eliminates length

$$\frac{Lg}{V^2} = \frac{1}{L} \times L = \text{zero dimensions}$$

$$= N_f \text{ (Froude number)}$$

$$F = F$$

Dividing by ρ eliminates force

$$\frac{F}{\rho} = \frac{F}{1} \times \frac{L^4}{FT^2} = \frac{L^4}{T^2}$$

Dividing by V^2 eliminates time

$$\frac{F}{\rho V^2} = \frac{L^4}{T^2} \frac{T^2}{L^2} = L^2$$

Dividing by L^2 eliminates length

$$\frac{F}{\rho V^2 L^2} = \frac{L^2}{L^2} = \text{zero dimensions}$$

$$= N_e \text{ (Euler number)}$$

The variables are now formed into dimensionless parameters which can be combined to give eq. 9, from which eq. 11 can be obtained as was done in the other two methods.

SUMMARY

The first method derives the dimensionless parameters in seven steps. For many problems this procedure is desirable when the user is not intimately familiar with the field in which he is working. The second method eliminates two steps from the first solution and derives the same parameters with greater ease. The ease by which the solution is made is based on the selection of the repeating variables and the arrangement of all the variables. This arrangement is dependent again on the knowledge of the user.

The third method is very simple and can be used merely by careful selection of the repeating variables and then forcing the remaining variables into dimensionless parameters. The parameters are identical to those found by the other two methods.

The three methods as presented are valid for finding dimensionless parameters and consequently functional equations in many different fields.

Journal of the
ENGINEERING MECHANICS DIVISION
Proceedings of the American Society of Civil Engineers

CONTENTS

DISCUSSION

DYNAMIC ELASTO-PLASTIC RESPONSE OF RIGID FRAMES[a]

Discussion by A. T. Matthews

A. T. MATTHEWS.[1]—In this paper the author presents an important contribution to the dynamic analysis of structures.

To illustrate this method of expansion into normal vibrational modes the dynamic response of a two-hinged rigid frame was obtained and carried up to the start of the second elasto-plastic phase. Regarding the assumptions and certain restrictions which are implied in this analysis the following observations may be made:

1. First elasto-plastic phase

In the example given, the location of the plastic hinge is assumed to be known, and it coincides with the position of maximum moment under static loading. It is true that hinges will form where the stress is maximum if the cross-section of the members is constant, and this in turn implies that hinges form at the location of maximum moments. However, under dynamic loading the effect of inertial forces may be such that maximum moments may occur at positions different from the static case. It is conceivable for certain types of two hinged frames that the maximum dynamic loading may not occur at the knee, even under the loading assumed by the author. However, using the author's method it is possible to determine the actual position of the maximum dynamic moments at the end of the first elastic phase. Therefore the initial hinge position need not be assumed or known previously. Also, it may be mentioned that, under some circumstances, it may be advisable to consider the effect of the axial forces in addition to moments in determining the position and time history of the hinges.

2. Subsequent elasto-plastic phases

Under transient loads of sufficiently long duration repeated elastic and elasto-plastic sequences may be anticipated, with hinge formation phenomena as discussed above. The author's method requires a new set of modes whenever a new plastic hinge occurs. In general the computational work of determining responses becomes impractical when many hinges form and re-form throughout the structure. Moreover, the location of these subsequent hinges requires knowledge of moments at all points at all times during the loading, and determination of these moments in the elasto-plastic phase requires summation of the second derivatives of displacements in each plastic mode. Poor convergence of such a series, as acknowledged by the author, restricts

a. Proc. Paper 1693, July 1958, by Frank L. DiMaggio.
1. Engr. Paul Weidlinger, Cons. Engr., New York, N. Y.

the moment determination to the first elasto-plastic phase of the motion. Therefore, this method is applicable to cases where the duration of the load is short compared to the period of the lowest elasto-plastic mode and gives practical engineering results for such cases.

In a recent paper by H. H. Bleich,(1) an alternative method is presented in which the original elastic modes are retained throughout the entire time history of the loading. For complex structures and for long duration loadings this results in a considerable reduction of the computational work and avoids some of the convergence problems.

REFERENCE

1. H. H. Bleich "Response of Elastoplastic Structures to Transient Loads," Section of Mathematics and Engineering, The New York Academy of Sciences, 1955.

Journal of the
ENGINEERING MECHANICS DIVISION
Proceedings of the American Society of Civil Engineers

THE RAPID DESIGN OF BEAMS IN TORSION

Cedric Marsh[1]

ABSTRACT

The design of beams in which torsion occurs, usually due to an eccentricity of the applied load, is either crudely approximated or, if studied accurately, involves the use of hyperbolic functions. This paper shows how simple beam formulas can be extended to deal with torsion and how, by considering torsional rigidity and torsion-bending rigidity separately, results of acceptable accuracy can be obtained.

Where primary torques are to be carried by structural members it is usual to employ shapes of the closed type, such as tubes or box beams, in which case analysis is relatively direct. When the twist arises due to the eccentricity of lateral loads, whose primary effect is bending, the shapes used will normally be of the standard I form, possibly augmented by channels fixed to one, or both flanges. This paper deals particularly with such shapes.

A structural shape resists twisting forces by a combination of torsional rigidity, defined by the term GJ, and torsion-bending rigidity defined by the term EH. In these terms, J is the torsion constant, H is the torsion-bending constant, E and G are the elastic and shear moduli.

In an I shape, that portion of the torque resisted by the torsional rigidity creates shear stresses as shown in Fig. 1a, while that portion resisted by torsion-bending creates shear stresses in the flanges (Fig. 1b) which are accompanied by longitudinal stresses as illustrated in Fig. 1c. These longitudinal stresses, as they are in addition to the longitudinal stresses caused by simple bending, are of first importance, and the following approximate analysis concerns itself specifically with these stresses. This treatment may also be used to give the deformation. Only in rare cases will the shear stress due to pure torsion in open sections govern before deformation becomes unacceptable.

Note: Discussion open until June 1, 1959. To extend the closing date one month, a written request must be filed with the Executive Secretary, ASCE. Paper 1923 is part of the copyrighted Journal of the Engineering Mechanics Division, Proceedings of the American Society of Civil Engineers, Vol. 85, No. EM 1, January, 1959.

1. Aluminum Co. of Canada, LTD., Montreal, Canada.

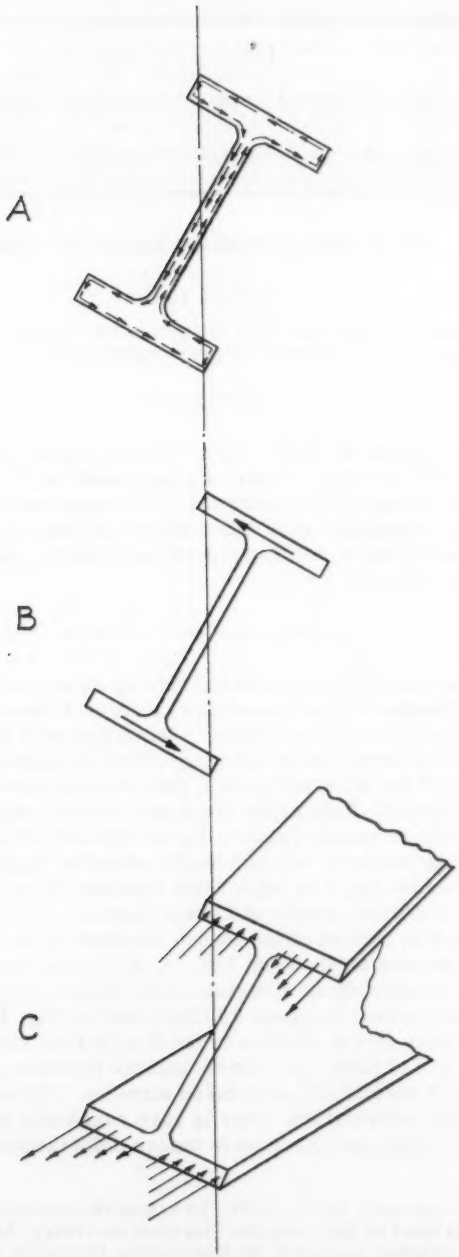

FIG. 1

Beam Analogy

To show the behaviour of a beam in torsion in terms familiar to engineers it is convenient to deal with torsion-bending and torsional rigidities independently.

Torsion-Bending

There is an exact analogy between the behaviour of a beam in bending and a beam resisting torques by torsion-bending only, as it does in stocky beams. (See appendix for the relevant relationships).

If the maximum bending moment and deflection in a beam are given by the terms:

$$M_b = C_m WL \qquad \text{and} \qquad \delta = C_\delta \frac{WL^3}{EI}$$

where C_m and C_δ are the appropriate constants,

W is the total load,

L is the span,

EI is the bending rigidity;

and the maximum stress is:

$$f_b = \frac{M_b h}{I}$$

where h is the distance from the centroid to the extreme fibre, then, for a beam subjected to a total torque, T, distributed in the same manner as W, the maximum torque-moment and rotation are:

$$M_t = C_m TL, \qquad \theta = C_\delta \frac{TL}{EH} \tag{1}$$

and the maximum longitudinal stress created by this torque is:

$$f_t = \frac{M_t D}{H} \tag{2}$$

where D is a geometric property of the shape, called here "unit warping," which is discussed later.

As an example, for a beam, with fixed ends, carrying a central load W:

$$M_b = \frac{WL}{8}, \qquad \delta = \frac{WL^3}{192EI},$$

and: -

$$f_b = \frac{WL}{8} \frac{h}{I}$$

In this case $C_m = 1/8$ and $C_\delta = \frac{1}{192}$, thus for a beam, with the flanges built in at the ends, carrying a central torque, T,:-

$$M_t = \frac{TL}{8}, \qquad \theta = \frac{TL^3}{192EH}$$

and the stress due to torsion-bending is:

$$f_t = \frac{TL}{8} \frac{D}{H}$$

If the load W is applied such that the distance from the shear center to the line of action of the load is e, the torque created on the member is We. Thus, it follows that, neglecting torsional rigidity, the ratio between the maximum stress due to the torque, We, and the stress caused by direct bending due to W, is simply:

$$\frac{f_t}{f_b} = \frac{De}{H} \Big/ \frac{h}{I}$$

In practice I/h is called the section modulus, S, and for convenience H/D will be called U, giving:

$$\frac{f_t}{f_b} = \frac{Se}{U} \qquad (3)$$

Pure Torsion

If, as in slender beams, the torsion-bending rigidity can be neglected and only the torsional rigidity is considered, the relevant laws governing stress and rotation will be analogous to those governing shear stress & shear deflection in a beam.

For example, a load W applied at the quarter point of a simply supported beam creates reactions of $\frac{3}{4}$ W and $\frac{1}{4}$ W, and a shear deflection of $\frac{3}{16} \frac{WL}{GV}$, where GV represents the shear rigidity of the beam. A torque T applied at a quarter point of a simple beam gives end torques of $\frac{3}{4}$ T and $\frac{1}{4}$ T and a rotation of $\frac{3}{16} \frac{TL}{GJ}$. (Although shear deflections are not usually calculated, and the formulas may be unfamiliar, the equations are simple enough to be computed directly. (Appendix b) is a table of some typical expressions for these deflections).

Combined Torsion and Torsion-Bending

Considered independently it is seen that the two modes of resisting torque follow relatively simple laws. The interaction of torsional and torsion-bending rigidity, however, involves a differential equation whose solution is in hyperbolic functions. To avoid this, it is here proposed that the partitioning of the torque between the torsional and torsion-bending components is made approximately by proportioning them directly in the ratio of the rigidities.

This means simply that if, under a total spplied torque T, the beam will rotate:

$$\theta_w = C_\delta \frac{TL^3}{EH}, \text{ if torsional rigidity is neglected,}$$

$$\text{or} \quad \theta_t = C_t \frac{TL}{GJ}, \text{ if torsion-bending rigidity is neglected,}$$

then the ratio of the torque carried by torsion-bending, T_w, to that carried by

pure torsion, T_t, is approximately:

$$\frac{T_w}{T_t} = \frac{\theta_t}{\theta_w} = \frac{C_t}{C_\delta} \frac{EH}{GJL^2}$$

Let $C_\delta / C_t = C$, and $GJL^2 / EH = a$, then if T is the total torque:

$$T_w = T/(1 + Ca) \tag{4}$$

The longitudinal stress due the torque T is then, from (1), (2) and (4):

$$f_t = \frac{C_m T}{(1 + Ca)} \frac{L}{U} \tag{5}$$

and the ratio between the longitudinal stress due to twisting caused by an eccentrically applied load and that due to bending, is:

$$\frac{f_t}{f_b} = \frac{Se}{U\ (1 + Ca)} \tag{6}$$

If the maximum deflection due to a load, W, is:

$$\delta = C_\delta\ WL^3 / EI$$

then the maximum rotation caused by its eccentricity, e, is:

$$\theta = C_\delta \frac{We}{(1 + Ca)} \frac{L^3}{EH}$$

and the total movement of the load is:

$$\delta + e\theta = C_\delta \frac{WL^3}{E} \left(\frac{1}{I} + \frac{e^2}{(1 + Ca)H} \right) \tag{7}$$

Shear Center

In shapes symmetrical about both axes, such as I beams, the shear center coincides with the centroid.

In channel shapes the shear center, lies on the x-x axis at a distance e behind the web, measured from the median line of the web (Fig. 2), given by:

$$e_c = \bar{x} \left(\frac{d}{2r_x} \right)^2$$

where d is the depth of the shape, measured between the median lines of the flanges, $\bar{x}$ is the distance from the median line of the web to the centroid, and r_x is the radius of gyration about the x-x axis. (See ref. 1 for the other shear center locations).

When two shapes are combined, the shear center lies at a point on the axis joining the shear centers of the individual shapes (Fig. 3) such that:

$$\frac{e_1}{e_2} = \frac{I_2}{I_1}$$

where I_1 and I_2 are the moments of inertia of the individual shapes about the axis on which the shear centers lie.

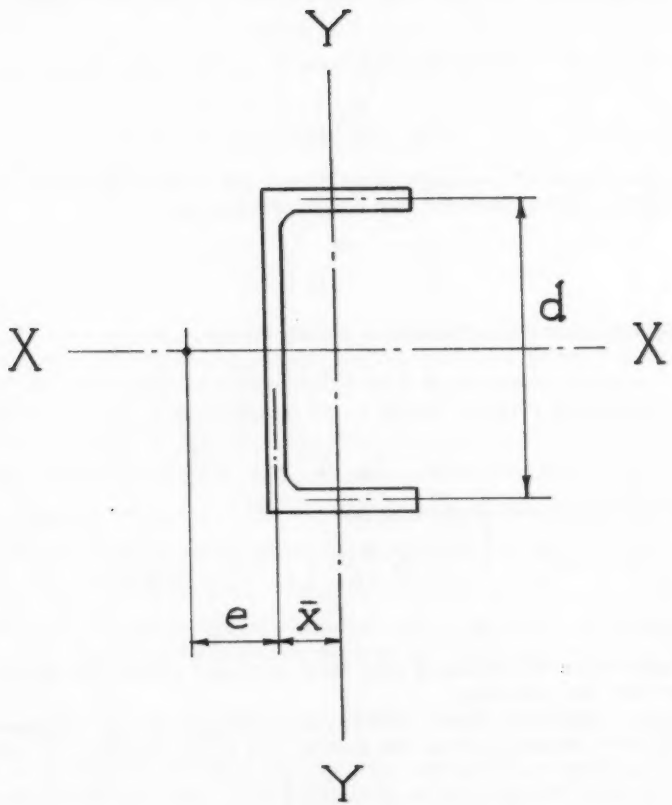

FIG. 2

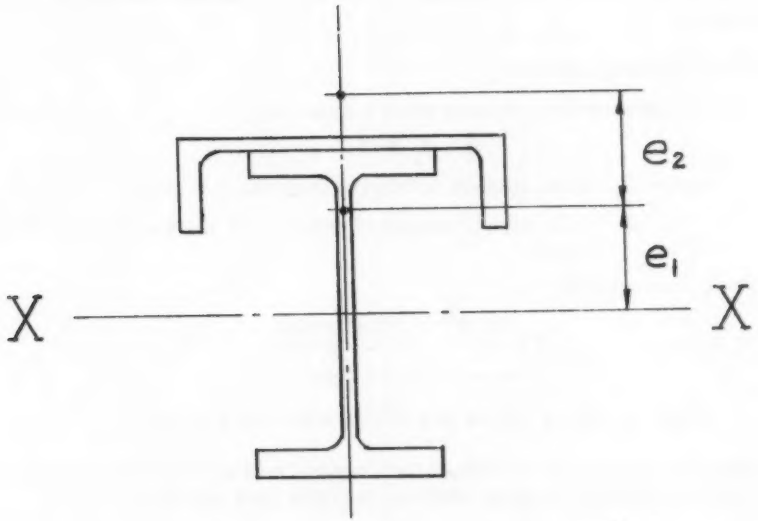

FIG. 3.

Torsion Constant

For a thin wall of breadth b and thickness t, the torsion constant is:

$$bt^3/3$$

The sum of these terms for all the individual walls will give a conservative approximation to the torsion constant of a shape. A more exact figure takes account of the influence of the roots fillets. For many standard shapes the values of the torsion constants are published[2,3] and the calculation is not necessary.

Torsion-Bending Constant

The torsion-bending constant of an I-shape is:

$$H = I_y d^2/4 \tag{10}$$

where I_y is the moment of inertia about the y-y axis,

d is the depth, measured between the median lines of the flanges.

For a channel (Fig. 2) =

$$H = \frac{I_y d^2}{4} \left(1 - \frac{\bar{x}(e - \bar{x})}{r_y^2}\right) \tag{11}$$

where r_y is the radius of gyration about the y-y axis.

When two shapes are combined the torsion-bending constant is equal to the sum of the individual torsion-bending constants plus the term:

$$Ie^2$$

for each individual shape, where e is the distance from the shear center of the individual shape to that of the complete section, and I is the moment of inertia of the individual shape about the axis joining the shear centers.

Torsion-Bending Stress

The stress created by torsion-bending results from the tendency of a cross section, which would have remained plane during simple bending, to "warp" out of plane under the action of a torque. The term "unit warping," D, is related to the maximum warping of the cross section from the original plane, or, if such warping is opposed, it is related to the maximum stress created.

The calculation of D will be illustrated by the example of an I-shape with a channel fixed to each flange (Fig. 4a).

The part ABC of the flange in Fig. 4a is opened out (Fig. 4b). This line is then treated as a beam subjected to a uniform load equal to the perpendicular distance from the shear center of the complete section to the median line of the wall in question (Fig. 4c). The total load on the beam is then reacted at the end representing the free edge of the flange by a force D. The shear stress in this fictitious beam (Fig. 4d) represents the distribution of stress in the flange due to torsion-bending, the maximum stress occuring at the free edge. In the other half of the flange the stress distribution is similar but of opposite sense.

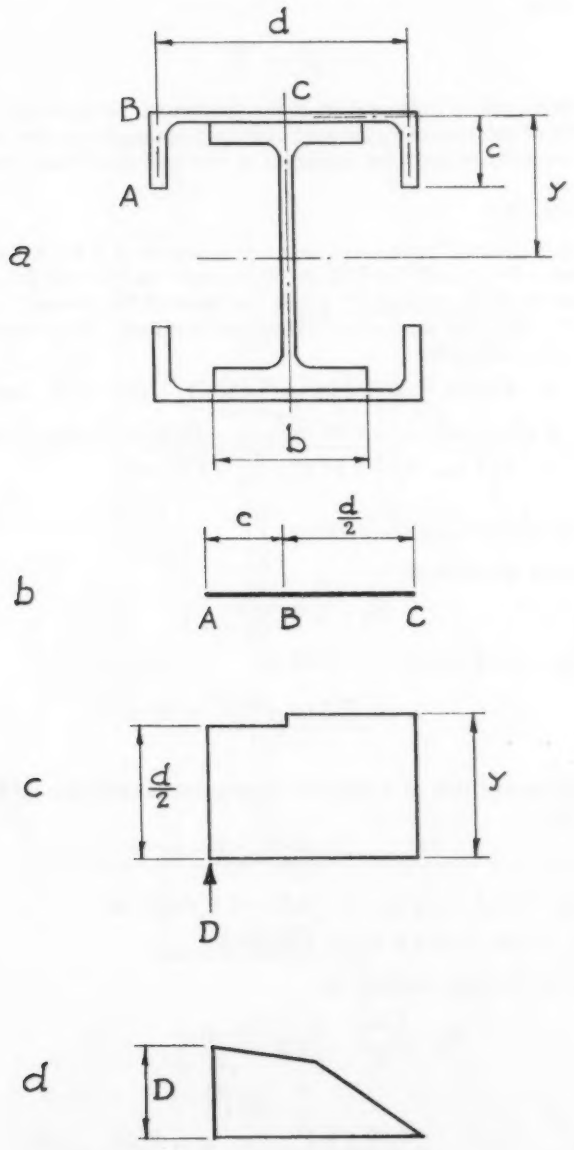

FIG. 4

In this case:

$$D = \frac{cd}{2} + \frac{dy}{2}$$

Note that this term is independent of the thickness. It is simply the sum of the products of the breadth of a wall and its distance from the shear center, such sum comprising only the material in one half of a flange assembly.

Example (Fig. 5).

A simply supported aluminum beam, comprised of a 9" x 4.33" x 7.51 lb/ft. I, with a 6" x 1.92" x 2.83 lb/ft. channel fixed to the top flange, carries a cental load W applied 2" above the back of the channel web, over a span of 80". Find the maximum stress and rotation: (For aluminum E = 10^7 psi, G = 4 x 10^6 psi).

I-shape $A = 6.38$ in.^{2}, $I_y = 5.09$ in.$^4 = I_1$, $I_x = 85.9$ in.^{4}, $J = 0.46$ in.^{4}

C-shape $A = 2.4$ in.^{2}, $I_y = 0.69$ in.^{4}, $I_x = 13.12$ in.$^4 = I_2$, $J = 0.088$ in.^{4}

$\bar{x} = 0.51$ in., $r_y = 0.54$ in., $r_x = 2.34$ in.

I-Shape

The shear center is at the centroid.

The warping constant is:

$$H_1 = I_y d_1^2/4$$

$$d_1 = 9 - 2 \times 0.29 = 8.42 \text{ in.}$$

$$\therefore H_1 = 5.09 \times \frac{8.42^2}{4} = 90 \text{ in.}^6$$

C-Shape

The shear center lies at a distance above the median line of the channel web, given by:

$$e_c = \bar{x}\,(d_2/2r_x)^2$$

$$d_2 = 6 - 0.4 = 5.6 \text{ in.}, \quad \bar{x} = 0.51 - 0.1 = 0.41 \text{ in.}$$

$$\therefore e_c = 0.41\,(5.6/2 \times 2.34)^2 = 0.59 \text{ in.}$$

The torsion-bending constant is:

$$H_2 = \frac{I_y d_2^2}{4}\left\{1 - \bar{x}\,\frac{(e-\bar{x})}{r_y^2}\right\}$$

$$= \frac{0.69 \times 5.6^2}{4}\left\{1 - 0.41\,\frac{(0.59 - 0.41)}{0.54^2}\right\} = 4.1 \text{ in.}^6$$

For the complete shape:

The distance between the individual shear centers is:

$$e^1 = 4.5 + 0.1 + 0.59 = 5.19 \text{ in.}$$

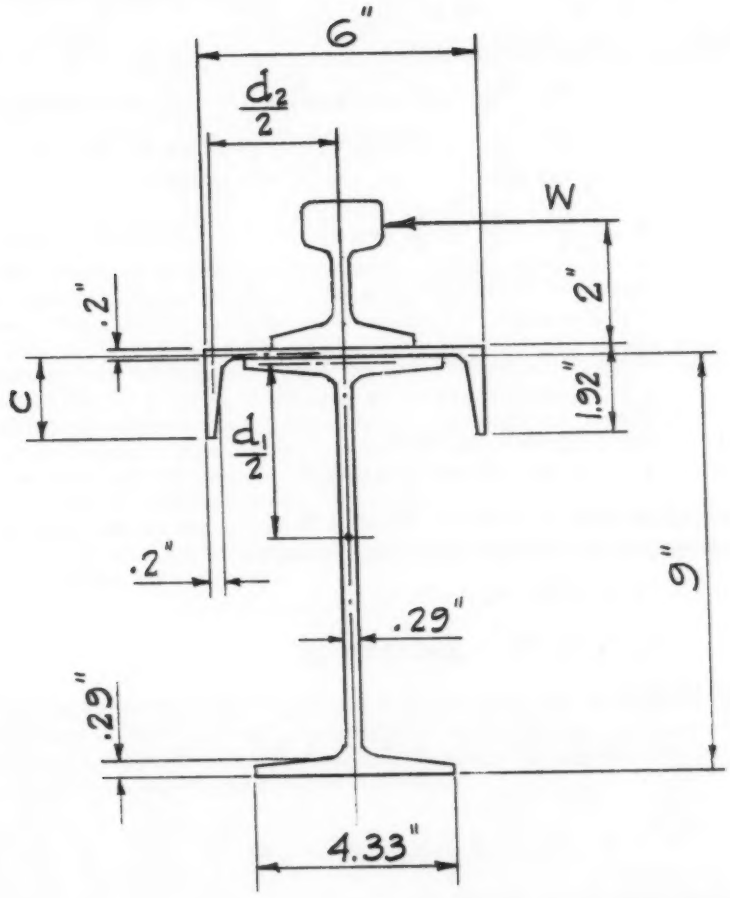

FIG. 5

The distance from the centroid of the I-shape to the shear center of the complete section:

$$e_1 = \frac{I_2}{I_1 + I_2} e^1 = \frac{13.12}{13.12 + 5.09} \times 5.19 = 3.7 \text{ in.}$$

The torsion-bending constant is then:

$$H = H_1 + H_2 + I_1 e_1^2 + I_2 e_2^2$$

$$= 90 + 4.1 + 5.09 \times 3.7^2 + 13.12 \times 1.49^2$$

$$= 193 \text{ in.}^6$$

$$D = \frac{cd}{2} + \frac{dy}{2} = \frac{d_2}{2} (c + y)$$

$$= 2.8 (1.82 + 0.9)$$

$$= 7.6 \text{ in.}^2$$

$$U = H/D = 193/7.6 = 25.4 \text{ in.}^4$$

$$I_y = 5.09 + 13.12 = 18.21 \text{ in.}^4$$

$$S_y = 18.21/3 = 6.07 \text{ in.}^3$$

$$J = 0.46 + 0.088 = .548 \text{ in.}^4$$

Eccentricity of load, e, = 6.7 - 3.7 = 3 in.

For a simply supported beam with a central load:

$$C_\delta = 1/48, \quad C_t = 1/4$$

$$C = C_\delta / C_t = \frac{1}{48} \Big/ \frac{1}{4} = \frac{1}{12}$$

For the member:

$$a = \frac{G}{E} \frac{JL^2}{H} = \frac{4}{10} \times \frac{0.548}{193} \times 80^2 = 7.3$$

Then:

$$(1 + Ca) = (1 + \frac{1}{12} \times 7.3) = 1.62$$

The stress due to direct bending is:

$$f_b = \frac{WL}{4S} = \frac{W \times 80}{4 \times 6.07} = 3.3W$$

The ratio of torsion-bending stress to bending-stress is:

$$\frac{f_t}{f_b} = \frac{Se}{U (1 + Ca)} = \frac{6.07 \times 3}{25.4 \times 1.62} = 0.443$$

giving a total stress of:

$$(1 + 0.443) \times 3.3W = 4.76W$$

The lateral deflection is:

$$\delta = \frac{WL^3}{48EI} = \frac{W \times 80^3}{48 \times 10^7 \times 18.2} = 0.59 \times 10^{-4} \text{ W in.}$$

The rotation at the center is:

$$\theta = \frac{WeL^3}{48\,(1 + Ca)EH} = \frac{W \times 3 \times 80^3}{48 \times 1.62 \times 10^7 \times 193} = 1.02 \times 10^{-4} \text{ W radians.}$$

and the total movement of the loaded point is then:

$$\delta + e\theta = (0.59 + 3 \times 1.02) \times 10^{-4} W$$
$$= 3.65 \times 10^{-4} \text{ W in.}$$

Accuracy of Method

The stress calculated by this method is most accurate for stocky beams. For a uniform load of constant eccentricity the error is negligible for all spans. For a central load, the error is small for values of "a" up to 1 and is -10% for "a" = 2, (as a percentage of the total stress it is appreciably less than this). As "a" becomes larger, deformation is more likely to govern design and errors in the computed stress are less significant.

Rotations computed in the above way are accurate for all values of "a" when the torque is distributed. A maximum error of approximately +10% occurs for a central torque when "a" lies between 3 and 4, the error approaching zero as "a" approaches zero or infinity.

To demonstrate the degree of accuracy, appendix c) is an example taken from ref. 2, re-worked using this approximate method, and the results compared with the exact answers.

CONCLUSION

As the values of torsion constants are published, and the torsion-bending properties of shapes can be computed from other published properties, the analysis of beams in torsion, using existing engineering formulas, is seen to be subject to a direct and practical treatment.

APPENDIX

a) The fundamental equations governing rotation in a member, due to applied torques opposed wholly by torsion - bending rigidity, are given below alongside those governing simple bending:

$$y'''' = -\frac{w}{EI} \quad , \quad \phi'''' = -\frac{t}{EH}$$

where t is the applied torque per unit length, analogous to the applied load, w.

$$y''' = -\frac{Q}{EI} \quad , \quad \phi''' = -\frac{\Gamma}{EH}$$

where Γ is the value of the torque at a point, analogous to the shear force, Q.

$$y'' = -\frac{M}{EI} \quad , \quad \phi'' = -\frac{M_t}{EH}$$

where M_t is here called the torque-moment, analogous to the bending movement, M.

$$y = -\iint \frac{M}{EI}\, dx^2 \quad , \quad \phi = -\iint \frac{M_t}{EH}\, dx^2$$

where ϕ is the rotation, analogous to the deflection, y.

Equations governing rotation created by torques opposed wholly by pure torsional rigidity, with those governing deflections due to shear, are given below.

$$y'' = -\frac{W}{GV} \quad , \quad y' = -\frac{Q}{GV} \quad , \quad y = -\int \frac{Q}{GV}\, dx$$

$$\phi'' = -\frac{t}{GJ} \quad , \quad \phi' = -\frac{\Gamma}{GJ} \quad , \quad \phi = -\int \frac{\Gamma}{GJ}\, dx$$

b) The maximum rotation, in members resisting a total applied torque by pure torsional rigidity, are given for some simple cases in the table below.

CASE	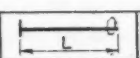	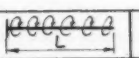	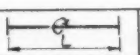	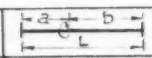	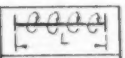
θ	$\frac{TL}{GJ}$	$\frac{TL}{2GJ}$	$\frac{TL}{4GJ}$	$\frac{Tab}{GJL}$	$\frac{TL}{8GJ}$

c) This example is one given in "Torsional Stresses in Structural Beams," Bethlehem Steel Corporation.

Simply supported 14WF74 spanning 20 ft. with a central vertical load of 22,000 lbs. at 2" eccentricity.

Effective depth, d = 13.4 in.,

Flange breadth b = 10.07 in., $D = d\,b/4 = 13.4 \times 10.07/4 = 33.7$ in.^{2}

$I_y = 133.5$ in.,^{4} $H = I_y \frac{d^2}{4} = 133.5 \times \frac{13.4^2}{4} = 6{,}000$ in.^{6}

$S_x = 112.3$ in.,^{3} $U = H/D = 6000/33.7 = 178$ in.^{4}

$J = 3.924$ in.^{4}

$E/G = 2.6$

$$a = \frac{G}{E}\frac{JL^2}{H} = \frac{1}{2.6} \times \frac{3.924 \times 240}{6000} = 14.5$$

C (from example 1) = 1/12

$(1 + Ca) = (1 + 14.5/12) = 2.21$

$$\frac{Se}{U\,(1 + Ca)} = \frac{112.3 \times 2}{178 \times 2.21} = 0.572$$

$$\text{Maximum Stress} = \frac{WL}{4S}\left\{1 + \frac{Se}{U\,(1 + Ca)}\right\} = \frac{22000 \times 240}{4 \times 112.3}\,(1 + 0.572)$$

$$= 18500 \text{ psi}$$

c.f. 19200 psi by exact method

$$\text{Maximum Rotation} = \frac{1}{48}\,\frac{We}{(1 + Ca)}\,\frac{L^3}{EH} = \frac{1}{48} \times \frac{22000 \times 2 \times 240^3}{2.21 \times 3 \times 10} \times 6000$$

$$= 0.031 \text{ radians}$$

c.f. 0.03 rads. by exact method.

REFERENCES

1. R. J. Roark, "Formulas for Stress and Strain" McGraw-Hill Book Company Inc.
2. Bethlehem Steel Corporation, "Torsional Stresses in Structural Beams."
3. Aluminum Company of America, "Structural Hardbook."
4. Timoshenko, "Theory of Bending, Torsion and Buckling of Thin-walled Members of Open Section," Journ. Franklin Institute - 1945.

NOMENCLATURE

A = cross sectional area of a shape, $in.^2$,

a = $\frac{GJL^2}{EH}$,

b = dimension of a shape, in.,

C = C_δ / C_t,

C_δ = constant in formula for bending deflection,

C_t = constant in formula for shear deflection,

c = a dimension of a shape, in.,

D = "unit warping," a geometric property of a shape to give torsion-bending stress, $in.^2$,

d = the depth of an I or channel shape measured between the median lines of the flanges, in.,

E = the elastic modulus, psi.,

e = a distance measured from the shear center, in.,

f_b = bending stress, psi.,

f_t = torsion-bending stress, psi.,

G = shear modulus, psi.,

H = torsion-bending constant for a shape, $in.^6$,

h = distance from the centroid to the extreme fibre of a shape, in.,

I = moment of inertia of a shape, $in.^4$,

J = torsion constant for a shape, $in.^4$,

L = span of a beam, in.,

M_b = maximum bending moment, lb. in.,

M_t = maximum torque-moment, lb. $in.^2$,

r = radius of gyration, in.,

S = section modulus of a shape, $in.^3$,

T = total applied torque, lb. in.,

T_t = torque carried by torsional rigidity, lb. in.,

T_w = torque carried by torsion-bending rigidity, lb. in.,

U = H/D, $in.^4$.

V = shear constant for a shape, $in.^4$,

W = total applied load, lb.,

$\bar{x}$ = a distance measured from the centroid, in.,

δ = maximum deflection, in.,

θ = maximum rotation, radians.

Γ = torque in a member, at a distance x from the origin, lb. in.